Growth and erosion rates of the East Carpathians volcanoes constrained by numerical models: Tectonic and climatic implications

S. Dibacto, P. Lahitte, D. Karátson, M. Hencz, A. Szakács, T. Biró, I. Kovacs, D. Veres

Growth and erosion rates of the East Carpathians volcanoes constrained by numerical models: tectonic and climatic implications

Dibacto, S.[1], Lahitte, P.[1], Karátson, D.[2], Hencz, M.[2], Szakács, A.[3], Biró, T.[2], Kovács, I.[4], Veres, D. [5]

[1]GEOPS, Univ. Paris-Sud, CNRS, Université Paris-Saclay, Rue du Belvédère, Bât. 504, 91405 Orsay, France

[2]Eötvös University, Department of Physical Geography, H-1117 Budapest, Pázmány s. 1/C, Hungary

[3]Department of Environmental Sciences, Sapientia University, Calea Turzii nr. 4, 400193 Cluj Napoca, Romania

[4]Geological and Geophysical Institute of Hungary, Geochemical and Laboratory Department, Stefánia út 14, 1143 Budapest, Hungary

[5]Institute of Speleology, Romanian Academy, Clinicilor 5, 400006 Cluj-Napoca, Romania

Abstract

The East Carpathian volcanic range experienced an along-arc, Late Miocene to Quaternary migration of eruptive activity during its ~11Ma-long activity. Here, a novel and complex methodology is presented that yields new geochronological and geomorphological constraints on the evolution of the 20 volcanic edifices. New unspiked K-Ar ages either constrain their lifespan (6.79±0.10 - 6.47±0.09 Ma for Seaca-Tătarca; 5.47±0.08 - 4.61±0.07 Ma for Vârghiş) or date the youngest volcanic activity (central Călimani). In parallel,

numerical reconstructions of volcanic paleo-topographies were performed to quantify their shape at the end of their construction stage. The inferred initial volcano size shows a wide range (3 to 592 km^3), making up the four main successive volcanic segments (910, 880, 279 and 165 km^3 for Călimani, Gurghiu, North Harghita and South Harghita segment, respectively) totalizing 2200 km^3 and an average growth rate of 200 km^3/Ma at range-scale. At the volcano-scale, with only consideration to their respective time spans (i.e. avoiding repose periods), growth rate is characterized by two major trends: a moderate growth rate (137 km^3/Ma) for the older volcanoes (11-3.6 Ma) followed by a lower growth rate (28 km^3/Ma) obtained for the Plio-Quaternary volcanoes. Comparing reconstructed and current topographies yielded a total eroded volume of 524±125 km^3, defining averaged denudation of 22% and a 20 m/Ma erosion rate. Erosion rates for major climatic periods were computed, which highlight the contrasting climatic contexts since 11 Ma. The highest erosion rate (38 m/Ma) occurred during transitional moderate subtropical-continental climate period (9.5-8.2 Ma). An intermediate erosion rate (14 m/Ma) characterized a moderate continental climate period (8.2-6.8 Ma) when conditions became less humid. The lowest erosion rate (7 m/Ma) reflects the prevailing continental but occasionally semi-arid climate (6.8-5.8 Ma). The highest erosion rate (28 m/Ma) was obtained for Plio-Quaternary times during the interglacial/glacial cycles. Such a quantitative morphometric and geochronological approach demonstrates its efficiency to study volcanic dynamism, including both constructional and erosional processes, through time.

Keywords

Numerical reconstruction; Volcano growth; Erosion rate; Paleo-climatic constraint

1 Introduction

A major geomorphological approach consists in assessing the time-dependent evolution of paleo and present topographies of landforms alongside the geological processes involved in their genesis, and, if possible, in numerically quantifying such processes (Leverington et al., 2002; Persson et al., 2004; Székely and Karátson, 2004; Wright et al., 2006; Grosse et al., 2009; Tucker and Hancock, 2010; Grosse et al., 2012; Karátson et al., 2012; Lahitte et al., 2012; Salvany et al., 2012). In volcanic fields with readily dateable topographic surfaces, one can constrain both dynamisms of volcanic growth and degrees of dismantling. Obviously, short-lived, recent, well datable volcanoes (i.e. of Late Quaternary age) can be studied with a high level of precision, whereas for older systems the precision will decrease. Growth and destruction of volcanoes may or may not be coupled, controlled by either endogenic (tectonic forces, volcanic eruptions) or exogenic processes (erosion controlled by climatic factors) (Thouret, 1999). A number of studies have aimed at constraining the total long-term erosion of volcanic surfaces using two approaches: 1) investigate long-lived but steady sourced volcanic systems such as stratovolcanoes based on edifice changes to track long-term erosional processes (Hildenbrand et al., 2008; Germa et al., 2011; Lahitte et al., 2012; Karátson et al., 2012; Salvany et al., 2012; Ricci et al., 2015a); and 2) study short-lived but dispersed small volcanic systems such as monogenetic volcanic fields using individual point-like data to extrapolate and understand the entire field behaviour (Kereszturi et al., 2013; Blaikie et al., 2015; Grosse et al., 2018). However, in the case of active volcanoes (with current eruption), a mass balance can be carried out either by quantifying the evolution of the topography of the volcano before, after, during and after the eruption or by carrying out a balance of the sediment load which is then reported on the surface of the watershed (Thouret et al., 2014). Digital elevation models (DEM) allow for characterizing the patterns of

68 erosion, and to extract geomorphic and structural information on large-volume edifices
69 which cannot be easily studied in the field (Favalli et al., 1999; Székely and Karátson,
70 2004). DEM-based quantitative geomorphological investigations enable the calculation of
71 constructed and/or eroded volumes and thus estimate magma output as well as erosion
72 rates. These, in turn, can be linked to hydroclimate variability driving the long-term erosion
73 processes: in the Carpathians, a humid continental climate (Karátson and Timár, 2005;
74 Karátson et al., 2019); in other areas with tropical and/or arid climates (Le Friant et al., 2004;
75 Samper et al., 2007; Hildenbrand et al., 2008; Germa et al., 2010, 2015; Karátson et al., 2012;
76 Lahitte et al., 2012; Salvany et al., 2012; Ricci et al., 2015a, 2015b; Bablon et al., 2018).
77 This study combines new geochronological constraints with a quantitative
78 geomorphological overview of the Călimani-Gurghiu-Harghita [1] volcanic range (hereafter
79 CGH, Fig. 1) in order to decipher its long-term topographic evolution. The unspiked
80 Cassignol-Gillot K-Ar technique has been used to obtain precise ages on four of the 17
81 volcanic centres (Central Călimani, Seaca-Tătarca, Vârghiş and Pilişca volcano). Also, we
82 performed DEM analysis to numerically model the paleo-topography of the volcanoes by
83 computing the best fitting surface to the volcanoes, making it possible to obtain constructed
84 and eroded volumes. Combining geomorphological information with available
85 geochronological data allow us to accurately assess the geomorphic evolution by calculating
86 growth and erosion rates, which in turn help constrain the timing and dynamism of
87 magmatic processes and to investigate links between tectonic and magmatic dynamism
88 (Wadge, 1982, 1984; Grosse et al., 2018).

[1] Official Romanian names are completed by locally used Hungarian names in Tables, also helpful for the reader to find names on local maps.

From cumulative erosion rates, computed at the scale of each volcano, we investigate their variations and how they correlate to the main climatic fluctuations under variegated but temperate continental climate-dominated conditions (Karátson, 1996), that the CGH area has experienced since the onset of volcanism started at 10.6 Ma (Pécskay et al., 1995).

2 Geological setting

The Carpathians are a major mountain range in Central and Eastern Europe spanning from Eastern Bohemia (Czech Republic), Poland, Slovakia, Hungary, Ukraine, to Romania and Serbia. Linked to the Alpine and Dinaric systems, they encompass the Pannonian and Transylvanian Basins (inset Fig. 1). Volcanic activity related to complex Tertiary to Quaternary geodynamic processes occurred both along the inner part of the Carpathian orogen and in the Carpatho-Pannonian Basin (Rădulescu and Săndulescu, 1973; Csontos et al., 1992; Szabó et al., 1992; Seghedi, 1995; Mason et al., 1996, 1998; Seghedi et al., 1998, 2004a, 2004b, 2005a, 2005b; Fielitz and Seghedi, 2005; Seghedi et al., 2019) .

Located in the eastern part of Romania's Inner Carpathians, the 160 km long CGH volcanic range constitutes the youngest, longest and southeasternmost segment of the Carpathian volcanic range (Fig. 1). The CGH is a typical post-collisional volcanic range as it developed after the stacking of the collision-related East Carpathian nappe system (Matenco and Bertotti, 2000). After the collision and the step-by-step propagation of the CGH volcanism parallel with the orogen, the plate boundaries more or less sealed. It was assumed to be associated with asthenosphere upwelling, explained by progressive break-off of an assumed Miocene subducted slab (Mason et al., 1998; Seghedi et al., 1998), as suggested by the present high heat flow coinciding exclusively with the volcanic area (Tari et al., 1999; Demetrescu et al., 2001). The CGH consists of a NW–SE-trending row of several adjoining

and partially overlapping volcanoes mostly characterized as composite volcanoes in the axial part and resulting from complex eruptive histories, including several cone-building phases interrupted by destruction phases (Szakács and Seghedi, 1995). The subduction-related, post-collisional volcanism (Rădulescu and Săndulescu, 1973; Pécskay et al., 1995; Seghedi et al., 2004a; Lexa et al., 2010) resulted in products which display calc-alkaline to alkaline compositions with andesite-dominated rock types (Mason et al., 1996, 1998; Seghedi et al., 2011). Volcanism of the overall CGH segment was interpreted as coeval with the last peak of crustal deformation in the Carpathian bend zone, characterized by uplift in the orogenic zone and subsidence in the foreland with amplitudes in the order of 2-4 km (Matenco et al., 2010).

3 Volcanism of the CGH range and its timing

The CGH volcanic range divides into four sub-segments corresponding respectively from the north to south to Călimani, Gurghiu, Northern and Southern Harghita (Fig. 1). As a result of the migration of volcanic activity along the range, the overlap between its 17 eruption centres is limited, allowing one to individualize them quite well. The first comprehensive study of CGH (Szakács and Seghedi, 1995, 1996) pointed out the systematic decrease of volume, height and width of the volcanic edifices from north (Călimani) to south (Southern Harghita), most of them surrounded by extended and partly coalesced volcaniclastic aprons.

The pre-volcanic basement of the CGH volcanic range belongs to two different major tectonic units, lithologically characterized by Proterozoic to Lower Palaeozoic metamorphic rocks overlain by Mesozoic, mostly carbonatic, sedimentary rocks of the East Carpathian's "Crystalline-Mesozoic Zone" in the eastern part (Săndulescu, 1988). A thick Paleogene-Neogene sedimentary pile including ductile rocks such as clay and salt prone to plastic

deformation (Ciupagea et al., 1970; Szakács and Krézsek, 2006) forms the pre-volcanic basement in the western part along the rim of the Transylvanian Basin. A topographic "anomaly" consisting in reverse-dipping (i.e. towards volcano center instead of towards volcano periphery) of the peripheral outer slopes of some volcanoes (e.g. Făncel-Lâpuşna and Seaca-Tătarca in Gurghiu Mts, and Vârghiş volcano in North Harghita, Fig. 1) was interpreted by Szakács and Krézsek (2006) as resulting from complex interactions between the pre-volcanic basement and the overlying volcanic edifices. Namely, the Late Miocene volcanoes grew up on a pre-volcanic basement including a thick salt layer which was squeezed-out, displaced and involved in enhanced diapirism governed by gravitational effects of the volcano loading. These processes modified in a certain degree also the original volcanic topography by volcano spreading (Delaney, 1992; Borgia, 1994; Merle and Borgia, 1996; Lagabrielle et al., 2000; Wooller et al., 2004; Borgia et al., 2005; Grosse et al., 2009, 2012), namely increasing edifice diameter and reducing relative height differences between volcano centre and periphery, hence reducing relief energy and erosion rates.

Available ages along the CGH range (Peltz et al., 1987; Szakács et al., 1993; Pécskay et al., 1995, 2006; Seghedi et al., 2004b, 2005; Karátson et al., 2019; Lahitte et al., 2019) defined a quasi-continuous eruptive activity from 10.6 to 0.03 Ma. The southwardly shift in eruption centres has been linked to progressive slab detachment following an oblique subduction stage (Mason et al., 1998; Seghedi et al., 1998).

For the past 10.6 Ma, the CGH range has been experiencing a temperate subtropical-continental climate with occasionally arid periods in the Late Miocene and a relatively humid climate with occasional periglacial regimes and interglacial/glacial variability during the Pliocene and Quaternary (Karátson, 1996; Fielitz and Seghedi, 2005; Magyari et al., 2014).

158 Details and evidence concerning climate changes in the Carpathian area are given in the
159 discussion.

160 4 Methods

161 4.1 K-Ar ages by unspiked Cassignol–Gillot technique

162 Seventeen new groundmass K-Ar ages are first presented here (Table 1). Results were
163 obtained on samples collected from four volcanoes representing the three main sectors of
164 the range (Călimani, Gurghiu, North and South Harghita). Measurements followed the
165 protocol of rock sampling, preparation and measurement as described by Germa et al.
166 (2011) and detailed in the supplementary materials (S.M.).

167 4.2 DEM-based volume calculations

168 Using a quantitative DEM-based approach of volumetry (Székely and Karátson, 2004;
169 Karátson and Timár, 2005; Favalli et al., 2009; Grosse et al., 2009; Kervyn et al., 2012; Lahitte
170 et al., 2012; Lavigne et al., 2013; Karátson et al., 2013; Germa et al., 2015; Ricci et al.,
171 2015a), we numerically modelled the paleo-topographies of all CGH volcanoes. To constrain
172 the shape that they displayed directly after the end of their respective activity, we follow the
173 method introduced by Lahitte et al. (2012) and improved since by Germa et al. (2015). The
174 resultant modelled volcanic surfaces are used to assess constructed and eroded volumes
175 (Ricci et al., 2015a), and then, using the available chronological data, to constrain the time-
176 space dynamism of volcano surface evolution through both construction and erosion rates.
177 To achieve our objectives, the topography of the CGH volcanic range was analysed from the
178 Shuttle Radar Topography Mission (SRTM) 30m-resolution DEM. Topographic surfaces were
179 modelled at 100m-resolution that compromises sufficient details of reconstruction and time

of calculation without affecting their quality (Wright et al., 2006; Grosse et al., 2009; Karátson et al., 2010; Kervyn et al., 2012).

4.2.1 Volcanic paleo-surface model

The main body of work relates to the topographic reconstruction of a volcano, i.e. the modelling of the surface that it reached after its growth ceased (the so-called pre-erosional volcanic surface, or PEVS). To model such surfaces, we use as input data the sectors of the current topography that still testify to the PEVS or, in other words, that have undergone ideally zero or minimal erosion since the volcano construction ceased. In detail, each grid cell of the present-day DEM was converted in a XYZ point, forming a huge input database (20 million points). Next, different morphometric parameters such as slope, topographic position index (TPI, Weiss, 2001) and topographic openness (TO, Yokoyama et al., 2002; Favalli and Fornaciai, 2017) were computed, assigned as attributes for each point and combined to select only points belonging to PEVS. These so-called constraining points (CPs) are commonly located on quasi-planar surfaces found commonly in the mid- to lower flanks of the volcanoes which, during long-term erosion, tend to be preserved relatively to the upper flanks and central parts that encompassed central depressions (Karátson et al., 2016; Favalli and Fornaciai, 2017). More than 200,000 CPs for the entire CGH volcanic range (Fig. 2A) were extracted. For practical reasons, they were reduced to one tenth without breaking the homogeneity of their distribution. The Seaca-Tătarca volcano (06 in Fig. 1) example is shown in Figure 3 to illustrate CPs extraction (purple dots in Fig. 2A, Fig. 3A and Fig. 3C) from its whole surface (green dots in Fig. 3A and coloured surface in Fig. 3C) and in consideration to slope, exposition, TO and TPI parameters. The elevation versus distance to centre diagram (Fig. 3A) highlights how CPs, independently of their position along the volcano profile (lower, mid or upper), belong to planezes surfaces, i.e. to the locally (at hundred-meter scale)

uppermost surface of the volcano. Note that only the main edifice was selected without considering the volcaniclastic materials of the ring plain immediately surrounding the central edifice (Zernack et al., 2011; Németh and Palmer, 2019). Finally, a careful visual control has been carried out in order to remove outlier points accidentally present in the ultimate CPs database. From their respective CPs, numerical reconstructions of 15 from the 16 selected volcanoes have been modelled using the ShapeVolc (SV) algorithm (Lahitte et al., 2012). Only Pilişca volcano (a small-sized shield volcano topped by a few lava domes in South Harghita; Szakács and Seghedi, 1995) has been reconstructed by the Kriging interpolation (Krige, 1951).

The ShapeVolc algorithm dedicated to volcano surface modelling was used successfully in various dismantling contexts: large flank collapse (Lahitte et al., 2012; Germa et al., 2015), caldera formation (Lavigne et al., 2013) or regressive erosion (Salvany et al., 2012; Ricci et al., 2015a, 2015b). This algorithm, as well as the one proposed by Favalli et al. (2014), fit the ideal surface by minimizing the mean square error between this surface elevation and those of the CPs.

ShapeVolc algorithm, assuming that a volcano displays at first order an axial symmetry (Karátson et al., 2012), finds, using the simplex algorithm, the set of parameters that define the first order geometry of a volume defined by a surface of revolution. Adjusted parameters are: XYZ coordinates of the axis of revolution (the location and elevation of the vent/summit); the elliptical shape of the edifice (i.e. the shape of its contour lines); and the parameters of the generatrix of the surface revolution (i.e. the function, black dots in Fig. 3B, that best fit the non-eroded upper volcanic surface**)**. As the current elevation of each CPs is the lowest one possible for the uppermost surface, parameters are calculated in order to

find the lowest possible surface of revolution passing above most of the CPs (see black curve relatively to purple dots in Fig. 3A).

A common way to model volcano shape and volume consists in a simple rotation of the best generatrix curve around an axis located at the volcano summit, defining a pure surface of revolution (Karátson et al., 2010, 2012). However, such kind of modelling does not consider the ellipticity of the volcano that is a common characteristic of edifices (Grosse et al., 2012, 2014; Favalli et al. 2014; Grosse and Kervyn, 2018). The observed improvement of results, when ellipticity is considered advocate for closely considering volcano eccentricity in our reconstructions (see details given in S.M.), has been done in this study: eccentricity and azimuth have been systematically computed.

Moreover, as taking into account the volcanic complexity of the surface is crucial to optimize precision in volume calculation, a major improvement is here introduced to allow ShapeVolc to take into account the second order of magnitude of details of volcanic surfaces. Indeed, if most volcanoes can be defined at first order by a mathematically defined, elliptical surface of revolution, the complexity of volcanic construction introduces heterogeneities on this mathematic perfection that commands modelling the second order of magnitude of their shape. Concretely, each PEVS model was performed in two steps. 1) The first order of magnitude of the volcanic surface was obtained by defining the unique set of parameters (listed above) that best fit to all CPs of the volcano. 2) The second step locally adjusts the surface to find elevation of each cell of the 100 m-resolution paleo-surface model with only considering the closest CPs of the given cell and selected by classical research criteria (typically the 20 nearest CPs in each of the eight 45°-large angular sectors). This time-consuming step (up to 120,000 elevation points to be modelled for a large volcano) allows for defining the uppermost PEVS and takes into account the irregularities of

the surface such as local elevation variations and small details in the volcanic structure (presence of parasitic and/or adventive cones or domes, such as Tarvez in Fig. 3A). This second order of detail becomes essential for young volcanoes where the very small amount of erosion material imposes the most adjusted surface as possible.

Uncertainty of our modelled volcano shapes (σZ_{SV}, Table 2) is calculated as the standard deviation of the difference (ΔZ_P) between the altitude of the constraining points (Z_{CP}) and the altitude of the modelled ones (Z_{SV}).

4.2.2 Volumetric data, growth and erosion rates

Estimating the volcano volume requires knowing the surface of its basement prior to its construction, the so-called pre-volcanic basal surface (PVBS). Details of PVBS modelling by kriging interpolation are given in the S.M.

Comparisons of pre-erosional volcano surface to PVBS and the present DEM allow calculations of constructed (V_C) or eroded (V_E) volumes, respectively. Next, the growth rates (GR, in km^3/Ma) defined by V_C divided by volcano lifespan (Δt) constrains the eruptive dynamism; the erosion rate (ER, in m/Ma) defined by V_E divided by the area and the erosion duration (i.e.; volcano age) and the degree of denudation (D_{Den}, the percentage of volcano volume removed by erosion), defined by V_E divided by V_C, are computed. Details of the modelling of PVBS and calculation of volumes and uncertainties, degree of denudation, growth and erosion rates are given in the S.M. The inferred erosion is highlighted in Fig. 3C by the black sticks that connect the present DEM as well as the PEVS surfaces.

Our reconstructions include both coherent and fragmented volcanic materials making up the edifices, and thus, they refer to bulk volumes instead of DRE (dense rock equivalent). Our constructed volumes and growth rates take into account the volcaniclastic aprons, but they are excluded from the V_E and ER since our calculations do not differentiate the

volcaniclastic aprons (their source and to which volcano they belong); so, an accurate proportioning is quasi-impossible. Our volcano GR differs from magma output rates sensu stricto as they only integrate a part of the whole pyroclastic material. However, it allows the obtaining of a general framework of magmatic activity through space and time along the CGH range and can be used as a good proxy for magma output rates (Wadge, 1982, 1984; Grosse et al., 2018).

5 Results

5.1 K-Ar ages

New K-Ar ages are reported in Table 1, with all uncertainties quoted at 1-sigma level (1σ). All Ar analyses were successfully duplicated at the 1σ level except sample 17EC14 that required a third measurement (see details of each measurement in the S.M.). Radiometric dating results are presented in chronological order in the following sections, compiled in Table 1 and discussed in Fig. 2A-D.

5.1.1 Călimani edifice

The four oldest dated samples of lava flows and intrusions belong to the Călimani caldera edifice. The oldest ages (8.30±0.12 and 8.33±0.12 Ma) were obtained on two distinct outcrops from the same andesite lava flow, illustratrating the good reproducibility of our dating method. The monzodioritic intrusion exposed in the central part of the Călimani caldera is slightly younger (8.26±0.12 Ma). In contrast, the dacitic lava dome at Pietricelul, built up on the Călimani caldera rim, constrains the post-caldera activity (6.69±0.10 Ma) and is comparable with the youngest ages measured previously in the Călimani area (Pécskay et al., 1995).

5.1.2 Seaca-Tătarca volcano (Gurghiu Mts.)

Five andesitic lava flows were dated on this large lava dominated volcano. Stratigraphical coherence is observed, as the oldest ages have been obtained on the innermost and lowest samples (6.65±0.09 and 6.79±0.10 Ma). Two intermediates ages were obtained from lava flows on the upper flanks of the volcano on the SSE and western sides (6.61±0.09 and 6.52±0.09 Ma, respectively). The youngest age was obtained on the uppermost rim of the erosional depression (6.47±0.09 Ma) in accordance with the relative stratigraphy. From the dated samples (that likely constrain the whole Seaca-Tătarca volcano stratigraphy), we infer a constructional period of ~330±140 ka.

5.1.3 Vârghiş volcano (North Harghita Mts.)

From the six andesite lava flows dated on the Vârghiş volcano, the oldest age (5.47±0.08 Ma) has been obtained on the only amphibole lava located in the lowest outcrop of the north sector of the central depression (identified as a sector-collapse depression by (Szakács and Seghedi, 1995, 2000). Two lava flows sampled inside the depression have provided intermediate ages (5.06±0.07 and 4.79±0.07 Ma) whereas two other (4.65±0.07 and 4.89±0.07 Ma) came from the upper flank of Harghita Mădăraş summit, described as a depression rim dome (Szakács and Seghedi, 1995). Finally, the post sector collapse and youngest activity is constrained at the southern periphery of the edifice (4.61±0.07 Ma). From these ages, we infer a constructional period of ~900±140 ka.

5.1.4 Pilişca volcano (South Harghita)

Two dacitic lava rocks from the Pilişca volcano (1.98±0.06 and 2.11±0.04 Ma) might represent late-stage dacitic lava domes stratigraphically overlying andesitic lavas of the early volcano stage located along the riverbed of the Olt river in the Tuşnad Gorge (2.11±0.03 and 2.13±0.03 Ma, in Karátson et al. 2019).

5.2 Volcanic surface models

5.2.1 Paleo-volcanic surfaces

From their constraining points (Fig. 2A), 16 CGH volcanoes were modelled (Fig. 4). Their morphometric characteristics are summarized in Table 2 (more exhaustively discussed in S.M.). They display two types of radial profile according to their main concave (modelled by an exponential or polynomial curve) or convex (gaussian curve) shape (Grosse et al., 2009). Ellipticity ranges from 0.16 (quasi-circular edifice) to 0.80 (strongly elongated one). Uncertainties of modelled surfaces range from 24 m to 82 m. Modelled volcanoes are characterized by contrasting sizes, from very small parasitic cones (Râchitis edifice, #12, 3±3 km^3) to large composite volcanoes (Central Călimani edifice, #01, 592±115 km^3; Fig. 1 and Fig. 4).

In the Călimani sector (Fig. 4A), the Central Călimani (#01, constituted by the current S and SE flanks of Rusca-Tihu and the associated cones of Lucaciul and Tămăul) and Moldovanul (#02) edifices have been reconstructed. They display contrasting shapes; the quasi-circular Central Călimani is best fitted by a concave shape (steep summit) whereas the more elliptical Moldovanul fits to a convex shape (relatively flat summit).

For Gurghiu sector (Fig. 4B), seven volcanoes have been modelled (#03 to #09, Fig. 4B). Whereas all have quite similar concave shape, four volcanoes (#03, #04, #05, #08) exhibit relatively high ellipticity (0.61-0.80) whereas the others are almost circular (0.16-0.37).

In North Harghita, all four modelled volcanoes (#10 to #13, Fig. 4C) display a marked ellipticity (0.33-0.80) and concave shape, except the very small Râchitis with a convex profile.

In South Harghita (Fig. 4D), the dual Luci-Lazu (#14a and #14b) and Cucu (#15) volcanoes display contrasting ellipticity (0.20 and 0.49, respectively) but both with quasi-linear profiles

(almost conical shape). Pilişca (#16), the youngest volcano in our study (only the late Pleistocene Ciomadul is younger in the whole CGH, Szakács and Seghedi, 1995; Karátson et al., 2019; Lahitte et al., 2019), has a such "un-geometric" shape that it requires kriging interpolation.

5.2.2 Volumetric results

Using the output from the geomorphological models, the main individual data for each volcano are compiled in Table 2 and comprise the area (A), Height, constructed (V_C) and eroded (V_E) volumes, growth (GR) and erosion (ER) rates and the degree of denudation (D_{Den}). To compute GR and ER, we considered all available radiometric ages from previous studies, most remaining conventional K-Ar ages being obtained on whole rock. For each volcano, we calculated an average age using as bracketing temporal constraints the oldest and youngest available ages and assuming that the average age represents the peak of activity.

The V_C computed for the 16 volcanoes modelled in this study ranges between 3±3 and 592±190 km^3. Fitting the volcano volume and area by a power-law function shows a good positive correlation (R^2=0.93; Fig. 5A) defined by:

$$V_c = 0.015 \times (A)^{1.51} \quad \text{Eq. 1}$$

We note that data on Fâncel-Lăpuşna (in Gurghiu) seems out of this general trend; however, its inclusion or exclusion from the analysis practically does not alter the correlation (R^2 remains 0.93). Dimensional analysis shows that volume and surface are related by a power-law function with a 1.5 exponent. For instance, a regular cone (radius R, height H, slope α) is defined as:

$$V = \tan(\alpha)/(3 \times \pi^{1/2}) \times A^{1.5} \quad \text{Eq. 2}$$

Using the computed volume and area of the 16 analysed volcanoes (some showing very irregular shapes due to emplacement above or around older ones and having different shapes, all displaying second order of magnitude, i.e. not a simple mathematical shape), we obtained roughly the same 1.5 correlation exponent between the two variables (Fig. 5A). We interpret this quasi-ideal correlation as the expression that, although each volcano experienced its own history of construction, the individual long-term growth was averaged out as a quite similar and common evolution along the range. Such a quantification approach, based on enhanced morphometry, can be considered as numerical validation of the trend predicted for arc volcanoes evolving from single cone to massif (Grosse et al., 2009).

Plotting the height versus volume diagram as proposed by Grosse et al. (2009) (Fig. 5A inset), they fall in the field of the massif trend which is coherent with the complexities of their topography and eruptive history. Furthermore, the power-law curve fitting CGH data in the height versus volume diagram (Fig. 5A inset) has a power exponent close to 1/3 (0.35). Again, this means, inversing the equation, that volume is almost related to height by a factor of three and confirms the more and less homomorphic shapes of all CGH volcanoes.

The V_E computed in this study ranges between 0.2 km^3 (Ciomadul) and 158±85 km^3 (Călimani), increasing toward the north of the range with ER range between 7 and 26 m/Ma. The degree of denudation of the studied volcanoes is in the range of 3–34% (the average weighted mean being 22%), which means that within the studied period (~11 Ma), less than one third of the original volcanic edifice has been removed by erosion.

Plotting the V_C against V_E shows a strong linear positive correlation with R^2=0.95 (black line, Fig. 5B) whereas D_{Den} values (expressed as percentages in Fig. 5B) do not systematically

391 fit with the V_C, i.e. small edifices (e.g. Bacta, Jirca, Moldovanul), as well as large ones
392 (Călimani, Fâncel-Lăpuşna) can display a high degree of denudation.

393 No correlation (r^2=0.01) exists between the degree of denudation (D_{Den}) and height (H)
394 (Fig. 6A) and, logically, with volume or area as they are strongly correlated. Additionally, no
395 effect on erosion by any altitudinal contrast appears. On the other hand, D_{Den} fit relatively
396 well with latitude (R^2=0.62, Fig. 6B). As morphometry of volcanoes cannot explain this fit,
397 other parameters such as age, spatial climate fluctuation, rock strength and edifice slope can
398 possibly drive this regional variation of the D_{Den} values. These aspects will be further
399 addressed in the discussion.

400 # 6 Discussion

401 ## 6.1 Volume comparison with previous results

402 Summarizing individually modelled constructional volumes (i.e. prior to erosion) leads to
403 a total original volcanic volume of 2240±190 km^3 in the CGH range during ~11 Ma, higher
404 than the 1400–1606 km^3 range previously proposed (Szakács et al., 1997; Karátson and
405 Timár, 2005; Seghedi et al., 2019) obtained with basic approaches. We interpret this higher
406 value compared to previous studies as due to the complete integration of erosionally
407 removed volumes over the whole edifice. Hence, our approach illustrates the importance of
408 reconstructing a full paleo-topography of the volcanic edifice, especially for heavily
409 dismantled volcanoes such as those in the Călimani and Gurghiu segment.

410 A clear anticorrelation exists between relative uncertainties of constructed volume
411 ($\sigma RELV_C$, range from 19% to 50%, details in S.M.) and average height (ΔH_{mean}, Fig. 7) and fits
412 particularly well (R^2=0.87) to an inverse function. Even if calculation of relative uncertainty is

obtained from a complex integration of elementary uncertainties over the whole area of the volcano, it can be approximated as

$$\sigma RELV_C \approx \text{sqrt}\left(\sigma_{Mean\_upper\_surface}^2 + \sigma_{Mean\_lower\_surface}^2\right) / \Delta H_{mean} \quad \text{Eq. 3}$$

where, ΔH_{mean} is the average elevation of the edifice, and both σ_{Mean} terms are the average uncertainties of the basal and upper surfaces. Consequently, for a given volume, the smaller the ΔH_{mean}, the more poorly constrained its average height, and the higher, the relative uncertainty associated to its reconstructed volume ($\sigma RELV_C$).

6.2 K-Ar age constraints

6.2.1 Comparison with previous radiometric age data

All new K-Ar ages (obtained on Central Călimani, Seaca-Tătarca, Vârghiş and Pilişca volcanoes, Table 1, Fig. 2A-D) match within 1σ with the previous, respective conventional K-Ar ages. As such, the main issue is not necessarily the absolute values but, rather, improving their precision, since the uncertainty has been reduced by a factor of 3 to 5 (typically around 0.1 Ma vs 0.4 Ma). This improvement is crucial for correctly defining the dynamism of the volcanism, which requires precise constraints on volcano lifespans.

The lifespan of Seaca-Tătarca volcano, for example, is shortened from a previous estimate of 1±0.4 Ma (Pécskay et al., 1995; Seghedi et al., 2004b) to 340±140 ka. For Vârghiş volcano, the new results slightly extend its youngest activity (4.61±0.07 Ma, this work, vs 4.9 Ma in Pécskay et al., 1995) and refine its relatively long lifespan from 0.7±0.4 to 0.9±0.1 Ma. For Pilişca volcano, newly dated units do not sufficiently encompass its full activity to allow constraining its lifespan based only on the new K-Ar ages.

6.2.2 Example of volcano growth through time: The case of Seaca-Tătarca volcano

The study of the well-defined, regular-shaped simple edifice of Seaca-Tătarca benefits from regularly distributed, well-dated samples, allowing for precisely correlating its volume growth rate through time (Fig. 8A and Fig. 8B), and proposes a growth model encompassing its whole construction phase. For this purpose, the dated samples are projected in a graph of elevation versus distance to centre, with correction of the ellipticity of the edifice (Fig. 8A). Next, considering the average topographic profile of the volcano at the end of its construction and assuming a homothetic construction (i.e. shape remains self-similar all the time), we computed the proportion of the volcano volume that was already constructed with constant growth rate when subsequent, dated lava flows erupted.

Based on this, the location of the oldest sample (17EC03) is calculated as corresponding to 10% of the construction of the edifice (Fig. 8A) which is consistent with its outcrop in the large, central erosive depression that has not yet sufficiently dismantled the innermost part of the volcano to reach its basement. Though coming from a lower elevation than the previous one, sample 17EC04, belongs to an upper section of the volcano (21% of the construction). It outcrops in a river valley whose topographic profile (represented by the lowest green dots in Fig. 8A) is less sloping than the volcanic sequence it crosscuts. Consequently, outcrops along this valley display younger and younger volcanic units toward the periphery of the volcano. Sample 17EC05 corresponds to an intermediate position during the construction of the edifice (65%) despite its location in the upper flanks. Indeed, as the volcano grew, its area increased, too, requiring more and more material to increase its elevation. Consequently, each new % of growth (i.e. elevation) occupied progressively lower thicknesses (in Fig. 8A, blue lines regularly spaced at 10% are closer and closer upward). The

uppermost and youngest dated lava flows (17EC02 and 17EC01, Fig. 8A) correspond almost to the last stage of the edifice construction (92% and 95%, respectively).

From these growth proportions through time (white dots in Fig. 8B), and assuming magma output rate as constant (straight line in Fig. 8B), we can define the growth pattern of the whole volcano. In particular, the age of the onset and end of its activity can be inferred as the time interval where the growth line intersects 0% and 100% of growth proportions, respectively. With consideration of uncertainties, this interpolation leads to a full construction of Seaca-Tătarca volcano from 6.80 Ma to 6.46 Ma (red dots in Fig. 8B) and, consequently, a lifespan of ~340 ka. Based on such detailed findings of a selected volcanic edifice, we can assume that detailed chronological studies on similar-sized volcanoes along CGH would result in faster growth rates as well.

6.3 Spatio-temporal evolution of the CGH volcanism

Compiling all available K-Ar ages (Fig. 9), i.e. the new unspiked K-Ar ages along with those on Ciomadul and Pilişca and the numerous conventional K-Ar ages, the previously recognized diachronism in volcanic activity along the CGH range can be confirmed, generally characterized by decreasing ages southward from the late Miocene (~ 11 Ma) volcanism in Călimani to the sub-recent (<0.1 Ma) activity at Ciomadul (Rădulescu and Săndulescu, 1973; Peltz et al., 1987; Szakács et al., 1993, 2018; Pécskay et al., 1995, 2006; Seghedi et al., 2004b; Seghedi et al., 2005; Karátson et al., 2019; Lahitte et al., 2019). However, detailed analysis along the range highlights overlaps in volcanic activity between some segments. In particular, the activity of Călimani and Gurghiu was partially simultaneous, roughly between 9.8 to 6.3 Ma (Seghedi et al., 2004b, 2005b; Pécskay et al., 2006). A second overlap is observed between the latest activity in Gurghiu and the early activity of North Harghita (6.3 - 5.1 Ma).

Detailed observation of southward age progression along the CGH range allows for observing various compartments in each segment (Fig. 9). For Călimani, volcanic activity was coeval in both edifices (Central Călimani and Moldovanul), the earliest activities starting in the northern area and then shifting southwards. This mechanism is highlighted by the trapezoid box in Fig. 9 illustrating how early activity started only in the north but subsequently took place simultaneously in the entire segment. In Gurghiu, also, southward age progression does not establish a real migration, but, instead, an extension of the volcanically active area (green trapezoid in Fig. 9). Isolating the oldest Gurghiu ages for each 20 km-large windows allows constraining its southward expansion (black line on Fig. 9). Starting from only Jirca's activity at the beginning, the volcanism experienced a widespread expansion of activity at a rate of 12.6 km/Ma (R^2=0.75) over the whole segment (all volcanic centres being active quasi contemporaneously). It seems that during this period, the volcanism reached its paroxysm and accounted for the main activity apparent at around 6.6 Ma (Fig. 10).

On the contrary, volcanism in North and South Harghita shows a well-defined southward migration. A full progression of ages can be observed toward the south, as activity in each subsequent volcanic centre generally begins at a progressively later date with relatively good correlations. Between 6.3 and 4.6 Ma, volcanism migrated at a rate of 13.4 km/Ma (R^2=0.72) over the whole North Harghita segment. Subsequently, from 4.3 to 0.03 Ma, volcanism continued to progress southward along South Harghita. Samples obtained for each volcanic centre show a narrow age range (typically <1 Ma), reflecting the migration of activity but at a slower rate (4.6 km/Ma, R^2=0.68; Fig. 9) than along the older parts of the CGH.

6.4 Growth rates evolution through time and tectonic implications

Combining ages with the new volume constraints allows for characterizing the major phases of volcanic activity, the quiescence periods and the evolution of magma output (Fig. 10A). To quantify this, the volume of each volcano is assumed to be erupted between the youngest and the oldest available ages, with a maximum output occurring at half-time of the age range (Grosse et al., 2018) and individual GR through time is defined, at volcano-scale, by a Gaussian-like curve (coloured curves in Fig. 10A). Next, summing all individual outputs through time, we computed cumulative growth rate (dashed grey line in Fig. 10A). Finally, the derivation of this curve gives the GR through time for the whole CGH volcanic activity (bold line in Fig. 10A). Even though the regional GR does not consider the possible subvolcanic bodies (see discussion in Karátson and Timár, (2005), it remains a good proxy for investigating overall magma output rate.

Starting around 11 Ma, the CGH range experienced three main periods of volcanic activity isolated by two long periods of relative quiescence (3.6–2.8 Ma and 1.5–0.9 Ma, Fig. 10A): first, a long and continuous period of activity between 10.6 to 3.6 Ma with a maximum pulse of activity at 6.6 Ma (contemporaneous to the growth of Seaca-Tătarca volcano); and next, a drastic decrease of volcanic activity with only episodic activities at 2.8–1.5 Ma and 1–0.03 Ma during the growth of Pilişca and Ciomadul. The migration of volcanism can be correlated to changes in the magma storage system (along with magma composition) influenced or triggered by changes in plate tectonic processes (see global context in Crisp, 1984; White et al., 2006; East Carpathian features in Mason et al., 1998; Seghedi et al., 2011). Before 3.6 Ma, most volcanoes (Fig. 10A, Fig. 10B and Fig. 10C) erupted relatively high volumes (>50 km^3) of basaltic andesite to andesite lavas with a typical calc-alkaline composition (Seghedi et al., 2011). Their homogeneous Sr-Nd-Pb isotopic composition may

528 reflect a common mantle source (Mason et al., 1996, 1998; Seghedi et al., 2011). On the
529 contrary, South Harghita volcanoes of the 3.6–0.03 Ma period (Fig. 10A and Fig. 10D) are
530 smaller (<30 km^3) and show different chemical composition with progressively increasing K-
531 content (from calc-alkaline to high-K calc-alkaline and shoshonite) and adakite-like features,
532 reflected by the increased proportions of dacites and shoshonites (Szakács et al., 1993;
533 Seghedi et al., 2011).

534 The two different magma sources should have been responsible for the observed
535 morphometric dichotomy in volcano size between the northern segments (from Călimani up
536 to Luci-Lazu edifice in North Harghita) and the three last edifices (Cucu, Pilişca, Ciomadul in
537 South Harghita). Such conclusions fit with observations of Crisp (1984) and White et al.
538 (2006), who showed that more mafic magmas are more easily mobilized in the lithosphere
539 and tend to erupt higher volumes (northern CGH volcanoes) than the differentiated ones
540 (i.e. most of South Harghita).

541 Subsequent GR values computed at segment-scale (234, 276, 116 and 39 km^3/Ma from
542 north to south segments, Table 2) as well as values at volcano-scale (>100 km^3/Ma until 3.6
543 Ma and <50 km^3/Ma after) clearly support the decrease of volcanic intensity along the range,
544 as previously identified by Szakács et al. (1995, 2018), and the effect of different magma
545 sources (Seghedi et al., 2011). Moreover, Bouguer and magnetic anomalies surveys (Seghedi
546 et al., 2019) revealed positive residual anomaly in the northern and axial part of the range,
547 indicating the presence of high-density subvolcanic bodies which may be correlated to the
548 high eruptive volumes computed in those segments. Contrarily, in the Southern Harghita,
549 residual magnetic anomalies are negative, indicating the presence of low-density structures
550 in coherence with the small volumes of volcanoes.

In Gurghiu segment, the main magmatic pulse of activity observed around 6.6 Ma (Fig. 10A) can be plausibly related to the migration of the subducted slab through the magma generating zone in the mantle and the initiation of the progressive detachment of the slab following an oblique subduction stage (Mason et al. 1998; Seghedi et al. 1998, 2011). This main pulse temporally coincides with an E–W compressional event that occurred across the entire Carpatho-Pannonian region during the late Miocene, interpreted as reflecting the arrival of thick and buoyant continental crust at the trench and its resistance to subduction (Peresson and Decker, 1997). Moreover, Gurghiu zone is mostly located at the intersection of regional tectonic elements with normal faults associated with paleo-basins (Seghedi et al., 2019). Interaction of tectonic structures would have created an area of low resistance, facilitating the penetration of magma and development of its ascent paths, thereby allowing rapid magma output and construction of large volcanic centres in this segment. Moreover, the largest positive magnetic anomaly identified under Gurghiu segment (Seghedi et al., 2019) was suggested to have been the solidified plumbing system responsible for generating the Seaca-Tătarca and Şumuleu volcanoes. Under a collisional regime, the progressive slab detachment toward the south (Fig. 10D) may have triggered gradual migration of magma production in South Harghita, along with emplacement of adjacent or overlapping volcanic structures (Mason et al., 1998; Seghedi et al., 2005b).

A decreasing volcano volume towards southeast (Szakács and Seghedi, 1995) (Fig. 4A; Table 2) can also be explained by the progressive opening of the lithospheric tear during slab steepening (Mason et al., 1998; Seghedi et al., 1998, 2011). Finally, during the final stages of subduction, a decrease in the convergence rate in the extreme south of the CGH (Fig. 10D) was evidenced (Seghedi et al., 2011), possibly also responsible for the smaller dimensions of the last three volcanoes.

The two Plio-Quaternary quiescence periods (3.6–2.8 and 1.5–0.9 Ma, Fig. 10A-D) were interpreted as linked to changes in magma sources by Seghedi et al. (2011). Interestingly, the 1.5–0.9 Ma time gap is a period when K-alkalic and Na-alkalic volcanism developed in other areas (shoshonites at Bixad/Malnaş and alkali-basalts in Perşani Mountains; Downes et al., 1995; Panaiotu et al., 2004).

Growth rate can be used as a good proxy for revealing the dynamism, fluctuation and intensity of volcanism. Globally, long-term eruption rates for silicic volcanism range from $<10^{-5}$ km^3/ka to 10^1 km^3/ka, the average being 2.3±0.8 km^3/ka for andesitic systems (Vidal and Bonneville, 2004; White et al., 2006). Plotting CGH growth rates results (Fig. 11) in the volcano volume versus lifespan graph of White et al. (2006) highlights two distinct magma output trends. The first group (most edifices of the three northernmost segments, plus Luci-Lazu volcano, blue symbols in Fig. 11) shows an average GR of 137 km^3/Ma. The second one (the three youngest Pliocene-Quaternary edifices of South Harghita plus a small Late Miocene edifice in Gurghiu, red symbols in Fig. 11) is characterized by five times lower GR (28 km^3/Ma).

Seaca-Tătarca volcano with the highest GR (825 km^3/Ma, yellow symbol in Fig. 11) remains isolated from these two trends. The exceptionally high GR value does not only originate from the high precision on dating results, which allows drastically refining its lifespan (340 ka). Indeed, even considering the typical 1 Ma-long lifespan computed for most northern CGH volcanoes, its GR would remain two times higher than the given general trend. This implies both an exceptionally intense dynamism of Seaca-Tătarca activity and the call for getting more accurate age results for other volcanoes, since the lifespan of most CGH volcanoes probably could be in the same order of magnitude.

598 Over the entire CGH range, the calculated average GR is 200 km^3/Ma (ratio between
599 total volume emitted by all volcanoes during the whole range lifespan ~11Ma, without
600 consideration of the repose periods), slightly larger than previously proposed 152-164
601 km^3/Ma range (Szakács et al., 1997; Karátson and Timár, 2005). Even if fluctuations in CGH
602 growth rate occurred through time (10-825 km^3/Ma), values remain low compared to values
603 for andesitic volcanoes (blue squares in Fig. 11 background) from other subduction-related
604 arcs (White et al., 2006). It testifies to the less intense magma generation processes in the
605 long term here than in areas where subduction is more intense, such as the West Indies,
606 Japan and the Andes (White et al., 2006). Again, higher-precision dating may result in more
607 intense GR at the lifetime scale of individual edifices as is the case with Seaca-Tătarca. Such a
608 finding matches with worldwide (real, short-term) GR values of composite cones such as at
609 Parinacota volcano, Chile (Hora et al., 2007).

610 ## 6.5 Erosion rate and degree of denudation through time

611 Summing eroded volumes of all CGH volcanoes gives a total of 524±125 km^3 (Table 2)
612 and an average D_{Den} of 22%, close to the 23% proposed by Karátson and Timár (2005). At
613 segment-scale, only the inferred eroded volume for Călimani segment (265±105 km^3) does
614 not match at 1σ with the previous results of Karátson and Timár (2005), the new value being
615 three times larger. The discrepancy, as presented above, rise from the difference in
616 estimation of pre-erosional volumes (V_C) that directly impact on the estimation of eroded
617 volumes.

618 At volcano-scale, the V_E vs V_C plot can be interpreted with respect to D_{Den} values as it is
619 the ratio between these two parameters (Fig. Fig. 5B). Volcanoes with different volumes but
620 experiencing the same D_{Den} rate (i.e. build at the more and less same period) would follow a
621 linear correlation with constant slope (dashed lines in Fig. Fig. 5B). South Harghita volcanoes

622 built during Plio-Quaternary present the lowest D_{Den} values (~17%); average D_{Den} reaches
623 20% for 5.1-6.8 Ma old volcanoes and 27% for the older ones (>7.1 Ma; Călimani and
624 northern volcanoes). On this graph, the vertical black arrows represent the additional of
625 erosion affecting the older volcanoes and relatively to the average behaviour of the younger
626 ones. This additional erosion increases with the volume of the volcano (bigger volcanoes
627 produced more eroded material). However, in CGH range, larger volcanoes are also mostly
628 the older ones, another parameter positively correlated to the V_E values (older volcanoes
629 suffered longer erosion leading to larger eroded volume). Therefore, as volcano size (V_C) and
630 age are globally positively correlated (Fig. 10A), these parameters sum these effects on V_E
631 behaviour (V_E=F(V_C)+G(Age)). Nonetheless, even if the amount of erosion (V_E) seems to be
632 nicely correlated to V_C, it is less relevant than the correlation between D_{Den} and the time
633 (dashed line in Fig. 5B). By averaging D_{Den} values (Table 2 and black dots in Fig. 12) on each
634 CGH segment leads to the following D_{Den} values: 30%, 25%, 20% and 15% (bottom of Table
635 2), confirming the progressive degradation of volcanoes toward north, as first quantified by
636 (Karátson, 1996).

637 Correlation of the D_{Den} versus time allows establishing relationships between erosion
638 rate (ER, i.e. aerial denudation or lowering of edifice height) and time. To better constrain
639 the fast evolution of D_{Den} for the early stage of dismantling, we added to the CGH volcanoes
640 dataset (this work, black dots in Fig. 12) the values proposed for the dozen edifices of the
641 Ciomadul volcanic complex dating to between 0.03 and 0.8 Ma (Karátson et al., 2019; Lahitte
642 et al., 2019, deduced D_{Den} summarised in supplementary material, grey dots in Fig. 12).

643 In the case of dismantling evolving through time according to a single behaviour, the
644 trend of D_{Den} would evolve from 0 at t=0 (no erosion right after the volcano construction) to
645 100% after an infinite duration (with any volcano completely eroded). In order to verify D_{Den}

646 (0) = 0, the best function to fit such behaviour is a reverse exponential function ($D_{Den}(t)=1 -$
647 $k.e^{-l.t}$), with k=1.

648 However, considering the exhaustive data set of denudation rate (0 to 11 Ma of
649 denudation duration) leads to a best fit function with k~0.9 that intersects the D_{Den} axis at
650 10% (dash blue line and y axis in Fig. 12). This means that a perfectly newly constructed
651 volcano would have already lost 10% by dismantling right after its construction. This leads to
652 an improvement of the D_{Den} behaviour, with the consideration of a more complex
653 dismantling history, during the first 1 Ma of the erosion, when erosion occurred
654 simultaneously to (and competed with) the growing volcano and just after the end of its
655 construction. It is highlighted by the fast denudation rates affecting the domes of the
656 Ciomadul complex (grey dots in Fig. 12), "instantaneously" erupted along the past 1 Ma. The
657 good correlation between their age (i.e. erosion lifespan) and D_{Den} values supports
658 interpretation of D_{Den} changes through time as better approximated by two distinct trends.
659 First, a very fast evolving trend in the early stage with D_{Den} evolving from 0 to 14% during
660 about the first 1 Ma (grey dots in Fig. 12). This trend also incorporates the proportion of the
661 volcano dismantled during its 0.4-1 Ma-long construction phase (with an average proportion
662 of 1% lost by 0.1 Ma-long lifespan). Then, a long-term (constrained by all other CGH
663 volcanoes) trend fitted by the following equation (inset Fig. 12; see supplementary material
664 for the detail of calculation):

665 $$D_{Den} = 1-0.89e^{-0.024t} \ (R^2=0.62) \text{ with t in Ma} \qquad \text{Eq. 4}$$

666 Namely, the first stage of erosion (the first hundred thousand years [0 - <0.4 Ma] and,
667 subsequently, with less intensity up to 0.8 Ma) is much more intense due to the presence of
668 unafforested slopes, unconsolidated material (and possibly the erosion pattern inherited

669 from the activity period of the volcano) which result in high erosion rates. It is followed by a
670 second slowly decelerating long-term trend that can be considered as steady-state erosion in
671 the <20 Ma window.

672 Reciprocally, the averaged through time erosion rate (red and orange dots in Fig. 12) is
673 fitted by a quickly decreasing function in the early stage, followed by a slowly decreasing
674 rate (red curve in Fig. 12) with R^2=0.72. Both cumulated ER and D_{Den} parameters support a
675 general behaviour that is time dependent.

676 In conclusion, our results fit with the already observed (Ruxton and McDougall, 1967;
677 Francis, 1983; Karátson, 1996; Karátson et al., 2012) changes in volcano degradation: a
678 short-term post-volcanic erosion (<0.8 Ma) was characterized by a rapid lowering and slope
679 dissection/valley formation of the edifices with relatively high ER (24-39m/Ma, Fig. 12),
680 followed by a drastic decrease until reaching an equilibrium stage, where erosion rate slowly
681 decrease as mainly operating through a well-established drainage network (Ollier and
682 Brown, 1971; Karátson, 1996; Karátson et al., 2012) (shown by the red curve based on
683 orange and red dots in Fig. 12).

684 On the other hand, within the long-term erosion, there are obvious changes in ER values
685 which can be linked to past climate variability. A crucial record for disentangling
686 hydrographic evolution in the Black Sea–Carpathian area from Late Neogene has been
687 provided by the marine core DSDP Site 380A (Leg 42B; Popescu, 2006). This record, along
688 with the long-term trend in the palynological steppe index curve (Traverse, 1978) which is a
689 proxy representative of past climate changes between cooler and warmer phases (Suc,
690 1984), indicates a continuously decreasing trend in warm and wet taxa for the Carpathian
691 area throughout Late Neogene and a strong variability during the Quaternary (Popescu,
692 2002, 2006).

693 However, ER is expected to depend on several factors in addition to climate conditions
694 such as lithology or edifice topography such as local slope (e.g. Cotton, 1952; Ollier and
695 Brown, 1971; Francis, 1983; Karátson et al., 1999; Thouret, 1999; Reiners et al., 2003). Again,
696 Fig. 6A clearly shows that morphometric parameters (e.g. height, area, volume) do not
697 control denudation; therefore, erosion of CGH volcanoes is mostly controlled by
698 hydroclimate variability and/or slope characteristics. For instance, Champagnac et al. (2014)
699 showed, based on mountainous relief with 10-35° slope, that the behaviour followed by
700 erosion over time can be approximated by a quadratic relationship. CGH volcanoes, with
701 typically 10-21° slopes (Karátson, 2007), fit well with this observation. Therefore, since
702 volcanoes in CGH present relatively uniform and moderate slopes and are largely dominated
703 by andesite composite volcano types, we suggest that the contrasts in erosion have been
704 mostly driven by past hydroclimate fluctuations with the relatively small impact of
705 topography and rock strength.
706 From the integrated erosion rate (ER) at segment-scale (17, 11, 9, 28 m/Ma in Călimani,
707 Gurghiu, North Harghita and South Harghita, respectively, Table 2), it is possible to infer the
708 ER that the main specific time intervals the CGH range experienced (Karátson, 1996;
709 Popescu, 2002, 2006; Erdei et al., 2007): 1) a short time period of subtropical-moderate
710 continental transitional climate (Late Miocene, ~9.5-8.2 Ma); 2) a moderate continental
711 climate with intervening semiarid periods (Late Miocene up to Pleistocene, ~8.2-4 Ma); and
712 3) a humid continental climate with periglacial regimes during the Pleistocene glaciations
713 (Late Pliocene-Quaternary, from ~3.0 Ma up to present). Knowing the cumulated ER of the
714 period t_1 and t_1+t_2, we computed the specific ER driving dismantling during the period t_2 that
715 leads to the cumulative ER of the period t_1+t_2. For instance, the cumulated ER for North
716 Harghita equals the erosion regime that specifically controlled the dismantling of North

717 Harghita before the construction of South Harghita plus the erosion regime during the
718 dismantling of South Harghita. Obviously, the ER calculated for a certain period allows
719 inferring the behaviour of erosion in response to prevailing climatic conditions.

720 This approach leads us to infer four successive erosion regimes showing a strong
721 fluctuation over time (Table 3 and large diamonds in Fig. 12). 1) The highest ER (38 m/Ma,
722 for the 10.8-6.9 Ma period, red diamond), obtained for the construction period of Călimani
723 (Fig. 12), fits with the influence of the transitional moderate subtropical-continental climate
724 period as defined above (Karátson, 1996; Popescu, 2002, 2006). 2) Decreasing ER for Gurghiu
725 (14 m/Ma, 8.7-5.5 Ma, green diamond) and North Harghita (7 m/Ma, 7.0-4.6 Ma, blue
726 diamond) accords with the subsequent, drastically decreased erosional processes
727 characterizing a moderate continental climate. The extremely low value of 7 m/Ma, pointed
728 out for Late Miocene to Pliocene times, can be explained by occasional semi-arid conditions
729 (Lisiecki and Raymo, 2005). Indeed, Pliocene was already characterized by long-term shifts
730 between the humid forest biotopes and run-off and the dry steppes, with changes linked to
731 large amplitude climatic and moisture variations (Suc, 1984; Popescu, 2002, 2006). 4) Finally,
732 the 28 m/Ma ER obtained for the Plio-Quaternary period (<3 Ma, yellow diamond) can
733 reflect the prevailing more humid conditions (Suc, 1984; Karátson, 1996; Popescu, 2002,
734 2006); Schreiber and Unger, 2006) with a minor impact of glacial erosive activity and
735 periglacial regime.

736 These results of erosion rate specific to the main time intervals analysed are following
737 reconstructions of variability in sea levels and progressively stronger land glaciations from
738 Late Neogene to recent times (Lisiecki and Raymo, 2005). These are correlated to a shift
739 from prevalent chemical weathering during Late Neogene to enhanced surface processes,
740 run-off and physical weathering prominent during the Quaternary (Gibbard and Lewin,

741 2009). The latter reflect rapid and high-amplitude successive hydroclimate variability
742 between humid and glacial periods (colder and generally drier periglacial conditions) and
743 shorter, wetter and warmer interglacials (Lisiecki and Raymo, 2005).

744 For the entire range, average ER is ~20 m/Ma, lower than the 31.5 m/Ma proposed by
745 Karátson (1996). The latter value was calculated for the highest crater-topped summit
746 regions only and consequently overestimated the average erosion rate over the whole area
747 as omitting the peripheral aprons affected by lower ER. Our calculated ER for the highest
748 volcanoes (Central Călimani, Fâncel-Lăpuşna, Seaca-Tătarca, Vârghiş and Şumuleu) give high
749 values (>14 m/Ma), whereas smallest edifices (Jirca, Bacta, Borzont, Râchitis, Pilişca) show
750 the lowest values (<11 m/Ma, Table 3), in accordance with these ages, the most elevated
751 (and larger in size) volcanoes are also the older ones.

752 Relying on inferences of past climatic variability for the broader Carpathian region and
753 experienced by the CGH range throughout its evolution (Traverse, 1978; Suc, 1984; Karátson,
754 1996; Popescu, 2002, 2006; Erdei et al., 2007), we suggest that the best way to express ER
755 variations is to detail them at the scale of an individual segment. Indeed, work at the scale of
756 the whole CGH would only propose a regional value without consideration of variations
757 through time, whereas work at the scale of a volcanic edifice would introduce local bias due
758 to the own history of construction/dismantling that each volcano experienced (even if the 16
759 ERs define a general trend).

760 Globally, few studies have investigated ER over a long-term period, hence the
761 relationship with the geodynamic context or past climate variability is still poorly understood
762 (Karátson and Timár, 2005; Germa et al., 2010; Karátson et al., 2012a; Smith et al., 2016).
763 Studies in tropical environments pointed out much higher ER (Louvat and Allègre, 1997;
764 Hildenbrand et al., 2008; Germa et al., 2010; Ricci et al., 2015b). The systematically higher ER

765 values support the dominant role of climate as a main factor during dismantling. Moreover,
766 differences in prevailing lithology can also affect the behaviour of ER. For example, basaltic
767 rocks experience a faster weathering compared to andesitic ones and hence show higher ER
768 (Gislason et al., 1996; Louvat and Allègre, 1997).

769 The termination of erosional processes on volcanic landforms is the complete
770 destruction of the volcano with a remnant morphology of necks and dykes (i.e. skeleton
771 stage: Cotton, 1952) and a D_{Den} reaching almost 100% (inset of Fig. 12). It defines a very
772 long-term stage (tens to hundreds of Ma) when the volcano is very slowly dismantled as ER
773 tend simultaneously to zero. The equation fitting D_{Den} long-term evolution (Eq. 4) leads to a
774 duration required to destroy 95% of the entire range of 120 -20/+50 Ma. Even if such
775 duration would be significantly modified by changes in the tectonic (e.g. uplift) and/or
776 climatic contexts (Peulvast and Claudino Sales, 2005), its order of magnitude is reliable given
777 some known relict morphologies that testify to Cretaceous or even older Mesozoic
778 volcanism (Klein, 1975; Sturt et al., 1979; Simon-Coinçon, 1989; Slingerland and Furlong,
779 1989).

780 # 7 Conclusions

781 From the modelled volcanic surfaces performed in this study, the constrained
782 constructed volumes allow classifying the CGH volcanoes in the field of volcanic massif,
783 which is in accordance with their topographic complexities and eruptive lifespan, as pointed
784 out by new ages of the Seaca-Tătarca (~340 ka) and Vârghiş (~900 ka) edifices. The 1/3-
785 exponent in the power-law function relying original heights and volume advocates for CGH
786 volcanoes as being self-similar, i.e. exhibiting homomorphic shapes irrespective of the
787 peculiar complexities of their constructional histories. The overall volume computed for the

788 entire CGH is ~2200 km^3, characterized by decreasing individual volumes from north to
789 south, matches the evolution in terms of influence from different magma sources and plate
790 tectonics. Individual growth rates per volcano distinguish a first moderate regime (137
791 km^3/Ma) for the majority of volcanoes (11-3.6 Ma), followed by a drastically decreased
792 output rate (28 km^3/Ma) for the mostly Plio-Quaternary volcanoes. Apart from these two
793 trends (representing the average of individual growth rate per volcano), the much higher GR
794 obtained for Seaca-Tătarca (825 km^3/Ma) is the consequence of probably both its shorter
795 activity (inferred from new K-Ar datings) and a stronger magmatic regime. However, this
796 finding also points out the poorly constrained duration of volcanic activity (and related
797 output rates) if computed from poorly constrained ages in the case of CGH volcanoes for
798 which modern standard dating is not yet available. Fluctuations of GR (relatively to the
799 moderate overall averaged value of 200 km^3/Ma) is interpreted as the manifestation of
800 strong fluctuations of volcanic activity driven by drastic changes in subduction mechanisms
801 with decrease of convergence rate during the Plio-Quaternary causing breakoff beneath
802 South Harghita and subsequent upwelling of asthenospheric mantle.
803 Beyond the average values of dismantling parameters (total eroded volume of 524±125
804 km^3, averaged denudation and erosion rate of 22% and 20 m/Ma, respectively), the
805 correlation established between denudation and time defines two contrasting intensities of
806 dismantling processes given their position along the erosional timeline. The first denudation
807 trend shows an intense and rapid denudation (< 0.8 Ma) after the cessation of volcanic
808 activity while the second long-term trend slows down over the remaining erosional lifespan.
809 Whereas this behaviour implies an almost constant erosion rate during the lifespan of the
810 CGH erosion, detailed erosion rate values computed for shorter time intervals evidence the
811 variety of intensity of erosion having occurred through time. Since volcanic edifices present

812 relatively uniform slopes and composition, these second order variations suggest that
813 contrasts of ER along CGH range were mostly driven by climate fluctuations through time:
814 highest ER (38 m/Ma) during the transitional moderate subtropical-continental climate
815 period; intermediate ER (14 m/Ma) characterizing a moderate continental climate period
816 when conditions became less humid; extremely low ER (7 m/Ma) coeval with continental,
817 but occasionally semi-arid, climate; and, finally, higher ER (28 m/Ma) when Plio-Quaternary
818 experienced generally wetter conditions with alternating glacial and interglacial stages.

819 The presented quantitative morphometric approach of paleo-volcanic landforms,
820 performed at the detailed scale of individual volcanoes, demonstrates the possibility of a
821 wide range of applications in various geological domains. They allow constraining
822 constructive processes of volcano-tectonic dynamism at the scales of both individual
823 volcanoes and global geodynamic context. Furthermore, by correlating eroded volumes and
824 climatic variations, the intensity of the processes driving the dismantling of the volcanic
825 range can also be well assessed.

826 ## Acknowledgments

827 We are particularly grateful to the two anonymous reviewers and Karoly Nemeth as well as
828 Editor Markus Stoffel for their comments and suggestions, which greatly helped us to
829 improve the clarity of this paper. This research has been supported by the Hungarian
830 Scientific Research Fund NKFIH-OTKA No. 765 K 115472 to DK. Financial support for SD and
831 PL was also provided by the SYSTER 2017 program 766 of INSU, CNRS. This is Laboratoire de
832 Géochronologie Multi-Techniques (LGMT) contribution number 155.

References

Bablon, M., Quidelleur, X., Samaniego, P., Le Pennec, J.-L., Lahitte, P., Liorzou, C., Bustillos, J.E., Hidalgo, S., 2018. Eruptive chronology of Tungurahua volcano (Ecuador) revisited based on new K-Ar ages and geomorphological reconstructions. Journal of Volcanology and Geothermal Research 357, 378–398. https://doi.org/10.1016/j.jvolgeores.2018.05.007

Blaikie, T.N., van Otterloo, J., Ailleres, L., Betts, P.G., Cas, R.A.F., 2015. The erupted volumes of tephra from maar volcanoes and estimates of their VEI magnitude: examples from the late Cenozoic Newer Volcanics Province, south-eastern Australia. Journal of Volcanology and Geothermal Research 301, 81–89.

Borgia, A., 1994. Dynamic basis of volcanic spreading. Journal of Geophysical Research: Solid Earth 99, 17791–17804. https://doi.org/10.1029/94JB00578

Borgia, A., Tizzani, P., Solaro, G., Manzo, M., Casu, F., Luongo, G., Pepe, A., Berardino, P., Fornaro, G., Sansosti, E., 2005. Volcanic spreading of Vesuvius, a new paradigm for interpreting its volcanic activity. Geophysical Research Letters 32.

Champagnac, J.-D., Valla, P.G., Herman, F., 2014. Late-Cenozoic relief evolution under evolving climate: A review. Tectonophysics 614, 44–65. https://doi.org/10.1016/j.tecto.2013.11.037

Ciupagea, D., Pauca, M., Ichim, T., 1970. Geology of the Transylvanian depression. Editura Academiei Republici Socialiste Romania, Bucharest.

Cotton, C.A., 1952. Volcanoes as landscape forms Whitcombe and Tombs. New Zealand.

Crisp, J.A., 1984. Rates of magma emplacement and volcanic output. Journal of Volcanology and Geothermal Research 20, 177–211. https://doi.org/10.1016/0377-0273(84)90039-8

Csontos, L., Nagymarosy, A., Horváth, F., Kovac, M., 1992. Tertiary evolution of the Intra-Carpathian area: a model. Tectonophysics 208, 221–241.

Delaney, P.T., 1992. You can pile it only so high. Nature 357, 194–196. https://doi.org/10.1038/357194a0

Demetrescu, C., Nielsen, S.B., Ene, M., Şerban, D.Z., Polonic, G., Andreescu, M., Pop, A., Balling, N., 2001. Lithosphere thermal structure and evolution of the Transylvanian Depression—insights from new geothermal measurements and modelling results. Physics of the Earth and Planetary Interiors 126, 249–267.

Downes, H., Seghedi, I., Szakács, A., Dobosi, G., James, D.E., Vaselli, O., Rigby, I.J., Ingram, G.A., Rex, D., Pécskay, Z., 1995. Petrology and geochemistry of late Tertiary/Quaternary mafic alkaline volcanism in Romania. Lithos 35, 65–81. https://doi.org/10.1016/0024-4937(95)91152-Y

Erdei, B., Hably, L., Kázmér, M., Utescher, T., Bruch, A.A., 2007. Neogene flora and vegetation development of the Pannonian domain in relation to palaeoclimate and palaeogeography. Palaeogeography, Palaeoclimatology, Palaeoecology 253, 115–140.

Favalli, M., Fornaciai, A., 2017. Visualization and comparison of DEM-derived parameters. Application to volcanic areas. Geomorphology 290, 69–84. https://doi.org/10.1016/j.geomorph.2017.02.029

Favalli, M., Innocenti, F., Pareschi, M.T., Pasquarè, G., Mazzarini, F., Branca, S., Cavarra, L., Tibaldi, A., 1999. The DEM of Mt. Etna: geomorphological and structural implications. Geodinamica Acta 12, 279–290.

Favalli, M., Karátson, D., Mazzarini, F., Pareschi, M.T., Boschi, E., 2009. Morphometry of scoria cones located on a volcano flank: A case study from Mt. Etna (Italy), based on high-resolution LiDAR data. Journal of Volcanology and Geothermal Research 186, 320–330. https://doi.org/10.1016/j.jvolgeores.2009.07.011

Favalli, M., Karátson, D., Yepes, J., Nannipieri, L., 2014. Surface fitting in geomorphology — Examples for regular-shaped volcanic landforms. Geomorphology 221, 139–149. https://doi.org/10.1016/j.geomorph.2014.06.009

Fielitz, W., Seghedi, I., 2005. Late Miocene–Quaternary volcanism, tectonics and drainage system evolution in the East Carpathians, Romania. Tectonophysics 410, 111–136. https://doi.org/10.1016/j.tecto.2004.10.018

Francis, H., 1983. Magmaandsediment-11 Problems of interpreting palaeovolcanics buried in the stratigraphiccolumn 19.

Germa, A., Lahitte, P., Quidelleur, X., 2015. Construction and destruction of Mont Pelée volcano: Volumes and rates constrained from a geomorphological model of evolution. Journal of Geophysical Research: Earth Surface 120, 1206–1226. https://doi.org/10.1002/2014JF003355

Germa, A., Quidelleur, X., Labanieh, S., Chauvel, C., Lahitte, P., 2011. The volcanic evolution of Martinique Island: Insights from K–Ar dating into the Lesser Antilles arc migration since the Oligocene. Journal of Volcanology and Geothermal Research 208, 122–135. https://doi.org/10.1016/j.jvolgeores.2011.09.007

Germa, A., Quidelleur, X., Labanieh, S., Lahitte, P., Chauvel, C., 2010. The eruptive history of Morne Jacob volcano (Martinique Island, French West Indies): Geochronology, geomorphology and geochemistry of the earliest volcanism in the recent Lesser Antilles arc. Journal of Volcanology and Geothermal Research 198, 297–310.

884 Gibbard, P.L., Lewin, J., 2009. River incision and terrace formation in the Late Cenozoic of Europe. Tectonophysics 474, 41–
885 55.

886 Gislason, S.R., Arnorsson, S., Armannsson, H., 1996. Chemical weathering of basalt in Southwest Iceland; effects of runoff,
887 age of rocks and vegetative/glacial cover. American Journal of Science 296, 837–907.

888 Grosse, P., Euillades, P.A., Euillades, L.D., de Vries, B. van W., 2014. A global database of composite volcano morphometry.
889 Bulletin of Volcanology 76, 784.

890 Grosse, P., Kervyn, M., 2018. Morphometry of terrestrial shield volcanoes. Geomorphology 304, 1–14.
891 https://doi.org/10.1016/j.geomorph.2017.12.017

892 Grosse, P., Orihashi, Y., Guzman, S.R., Sumino, H., Nagao, K., 2018. Eruptive history of Incahuasi, Falso Azufre and El Condor
893 Quaternary composite volcanoes, southern Central Andes. Bulletin of Volcanology 80, 44. https://doi.org/10.1007/s00445-
894 018-1221-5

895 Grosse, P., van Wyk de Vries, B., Euillades, P.A., Kervyn, M., Petrinovic, I.A., 2012. Systematic morphometric
896 characterization of volcanic edifices using digital elevation models. Geomorphology 136, 114–131.
897 https://doi.org/10.1016/j.geomorph.2011.06.001

898 Grosse, P., van Wyk de Vries, B., Petrinovic, I.A., Euillades, P.A., Alvarado, G.E., 2009. Morphometry and evolution of arc
899 volcanoes. Geology 37, 651–654. https://doi.org/10.1130/G25734A.1

900 Hildenbrand, A., Gillot, P.-Y., Marlin, C., 2008. Geomorphological study of long-term erosion on a tropical volcanic ocean
901 island: Tahiti-Nui (French Polynesia). Geomorphology 93, 460–481. https://doi.org/10.1016/j.geomorph.2007.03.012

902 Hora, J.M., Singer, B.S., Wörner, G., 2007. Volcano evolution and eruptive flux on the thick crust of the Andean Central
903 Volcanic Zone: 40Ar/39Ar constraints from Volcán Parinacota, Chile. Geological Society of America Bulletin 119, 343–362.

904 Karátson, D., 2007. A Börzsönytől a Hargitáig—vulkanológia, felszínfejlődés, ősföldrajz. Typotex Kiadó, Budapest 463.

905 Karátson, D., 1996. Rates and factors of stratovolcano degradation in a continental climate: a complex morphometric
906 analysis for nineteen Neogene/Quaternary crater remnants in the Carpathians. Journal of Volcanology and Geothermal
907 Research 73, 65–78. https://doi.org/10.1016/0377-0273(96)00016-9

908 Karátson, D., Favalli, M., Tarquini, S., Fornaciai, A., Wörner, G., 2010. The regular shape of stratovolcanoes: A DEM-based
909 morphometrical approach. Journal of Volcanology and Geothermal Research 193, 171–181.
910 https://doi.org/10.1016/j.jvolgeores.2010.03.012

Karátson, D., Telbisz, T., Dibacto, S., Lahitte, P., Szakács, A., Veres, D., Gertisser, R., Jánosi, Cs., Timár, G., 2019. Eruptive history of the Late Quaternary Ciomadul (Csomád) volcano, East Carpathians, part II: magma output rates. Bulletin of Volcanology 81. https://doi.org/10.1007/s00445-019-1287-8

Karátson, D., Telbisz, T., Harangi, S., Magyari, E., Dunkl, I., Kiss, B., Jánosi, C., Veres, D., Braun, M., Fodor, E., 2013. Morphometrical and geochronological constraints on the youngest eruptive activity in East-Central Europe at the Ciomadul (Csomád) lava dome complex, East Carpathians. Journal of Volcanology and Geothermal Research 255, 43–56.

Karátson, D., Telbisz, T., Woerner, G., 2012. Erosion rates and erosion patterns of Neogene to Quaternary stratovolcanoes in the Western Cordillera of the Central Andes: An SRTM DEM based analysis. Geomorphology 139, 122–135. https://doi.org/10.1016/j.geomorph.2011.10.010

Karátson, D., Thouret, J.-C., Moriya, I., Lomoschitz, A., 1999. Erosion calderas: origins, processes, structural and climatic control. Bulletin of Volcanology 61, 174–193. https://doi.org/10.1007/s004450050270

Karátson, D., Timár, G., 2005. Comparative volumetric calculations of two segments of the Carpathian Neogene/Quaternary volcanic chain using SRTM elevation data: implications for erosion and magma output rates, in: Thouret, J.C., Chester, D.K. (Eds.), Volcanic Landforms, Processes and Hazards. pp. 19–35.

Karátson, D., Yepes, J., Favalli, M., Rodriguez-Peces, M.J., Fomaciai, A., 2016. Reconstructing eroded paleovolcanoes on Gran Canaria, Canary Islands, using advanced geomorphometry. Geomorphology 253, 123–134. https://doi.org/10.1016/j.geomorph.2015.10.004

Kereszturi, G., Németh, K., Cronin, S.J., Agustín-Flores, J., Smith, I.E., Lindsay, J., 2013. A model for calculating eruptive volumes for monogenetic volcanoes—Implication for the Quaternary Auckland Volcanic Field, New Zealand. Journal of Volcanology and Geothermal Research 266, 16–33.

Kervyn, M., Ernst, G.G.J., Carracedo, J.-C., Jacobs, P., 2012. Geomorphometric variability of “monogenetic” volcanic cones: evidence from Mauna Kea, Lanzarote and experimental cones. Geomorphology 136, 59–75.

Klein, C., 1975. Massif armoricain et bassin parisien: contribution à l’étude géologique et géomorphologique d’un massif ancien et de ses enveloppes sédimentaires: Normandie, Maine, Anjou, Touraine, Poitou septentrional et contrées adjacentes. Fondation Baulig.

Krige, D.G., 1951. A statistical approach to some basic mine valuation problems on the Witwatersrand. Journal of the Southern African Institute of Mining and Metallurgy 52, 119–139.

Lagabrielle, Y., Guivel, C., Maury, R.C., Bourgois, J., Fourcade, S., Martin, H., 2000. Magmatic–tectonic effects of high thermal regime at the site of active ridge subduction: the Chile Triple Junction model. Tectonophysics 326, 255–268.

Lahitte, P., Dibacto, S., Karátson, D., Gertisser, R., Veres, D., 2019. Eruptive history of the Late Quaternary Ciomadul (Csomád) volcano, East Carpathians, part I: timing of lava dome activity. Bulletin of Volcanology 81. https://doi.org/10.1007/s00445-019-1286-9

Lahitte, P., Samper, A., Quidelleur, X., 2012. DEM-based reconstruction of southern Basse-Terre volcanoes (Guadeloupe archipelago, FWI): Contribution to the Lesser Antilles Arc construction rates and magma production. Geomorphology 136, 148–164. https://doi.org/10.1016/j.geomorph.2011.04.008

Lang, B., Edelstein, O., Steinitz, G., Kovacs, M., Halga, S., 1994. Ar-Ar dating of adularia; a tool in understanding genetic relations between volcanism and mineralization; Baia Mare area (Gutii Mountains), northwestern Romania. Economic Geology 89, 174–180. https://doi.org/10.2113/gsecongeo.89.1.174

Lavigne, F., Degeai, J.-P., Komorowski, J.-C., Guillet, S., Robert, V., Lahitte, P., Oppenheimer, C., Stoffel, M., Vidal, C.M., Surono, Pratomo, I., Wassmer, P., Hajdas, I., Hadmoko, D.S., de Belizal, E., 2013. Source of the great A.D. 1257 mystery eruption unveiled, Samalas volcano, Rinjani Volcanic Complex, Indonesia. Proc Natl Acad Sci USA 110, 16742. https://doi.org/10.1073/pnas.1307520110

Le Friant, A., Harford, C.L., Deplus, C., Boudon, G., Sparks, R.S.J., Herd, R.A., Komorowski, J.C., 2004. Geomorphological evolution of Montserrat (West Indies): importance of flank collapse and erosional processes. Journal of the Geological Society 161, 147–160. https://doi.org/10.1144/0016-764903-017

Leverington, D.W., Teller, J.T., Mann, J.D., 2002. A GIS method for reconstruction of late Quaternary landscapes from isobase data and modern topography. Computers & Geosciences 28, 631–639.

Lisiecki, L.E., Raymo, M.E., 2005. A Pliocene-Pleistocene stack of 57 globally distributed benthic δ18O records. Paleoceanography 20.

Lexa, J., Seghedi, I., Nemeth, K., Szakács, A., Konecny, V., Pécskay, Z., Fueloep, A., Kovacs, M., 2010. Neogene-Quaternary Volcanic forms in the Carpathian-Pannonian Region: a review. Central European Journal of Geosciences 2, 207-U75. https://doi.org/10.2478/v10085-010-0024-5

Louvat, P., Allègre, C.J., 1997. Present denudation rates on the island of Réunion determined by river geochemistry: Basalt weathering and mass budget between chemical and mechanical erosions. Geochimica et Cosmochimica Acta 61, 3645–3669. https://doi.org/10.1016/S0016-7037(97)00180-4

Magyari, E.K., Veres, D., Wennrich, V., Wagner, B., Braun, M., Jakab, G., Karatson, D., Pal, Z., Ferenczy, G., St-Onge, G., Rethemeyer, J., Francois, J.-P., von Reumont, F., Schaebitz, F., 2014. Vegetation and environmental responses to climate forcing during the Last Glacial Maximum and deglaciation in the East Carpathians: attenuated response to maximum cooling and increased biomass burning. Quaternary Science Reviews 106, 278–298. https://doi.org/10.1016/j.quascirev.2014.09.015

Mason, P.R.D., Downes, H., Thirlwall, M.F., Seghedi, I., Szakács, A., Lowry, D., Mattey, D., 1996. Crustal Assimilation as a Major Petrogenetic Process in the East Carpathian Neogene and Quaternary Continental Margin Arc, Romania. Journal of Petrology 37, 927–959. https://doi.org/10.1093/petrology/37.4.927

Mason, P.R.D., Seghedi, I., Szákacs, A., Downes, H., 1998. Magmatic constraints on geodynamic models of subduction in the East Carpathians, Romania. Tectonophysics 297, 157–176. https://doi.org/10.1016/S0040-1951(98)00167-X

Matenco, L., Bertotti, G., 2000. Tertiary tectonic evolution of the external East Carpathians (Romania). Tectonophysics 316, 255–286.

Matenco, L., Krézsek, C., Merten, S., Schmid, S., Cloetingh, S., Andriessen, P., 2010. Characteristics of collisional orogens with low topographic build-up: an example from the Carpathians. Terra Nova 22, 155–165. https://doi.org/10.1111/j.1365-3121.2010.00931.x

Merle, O., Borgia, A., 1996. Scaled experiments of volcanic spreading. Journal of Geophysical Research: Solid Earth 101, 13805–13817. https://doi.org/10.1029/95JB03736

Molnár, K., Harangi, S., Lukács, R., Dunkl, I., Schmitt, A.K., Kiss, B., Garamhegyi, T., Seghedi, I., 2018. The onset of the volcanism in the Ciomadul Volcanic Dome Complex (Eastern Carpathians): Eruption chronology and magma type variation. Journal of Volcanology and Geothermal Research 354, 39–56. https://doi.org/10.1016/j.jvolgeores.2018.01.025

Németh, K., Palmer, J., 2019. Geological mapping of volcanic terrains: Discussion on concepts, facies models, scales, and resolutions from New Zealand perspective. Journal of Volcanology and Geothermal Research 385, 27–45.

Ollier, C.D., Brown, M.J.F., 1971. Erosion of a young volcano in New Guiana. Zeitschrift fur Geomorphologie 15, 12–28.

Panaiotu, C.G., Pécskay, Z., Hambach, U., Seghedi, I., Panaiotu, C.E., Tetsumaru, I., Orleanu, M., Szakács, A., 2004. Short-lived quaternary volcanism in the Persani Mountains (Romania) revealed by combined K-Ar and paleomagnetic data. Geologica Carpathica 55, 333–339.

Pécskay, Edelstein, O., Seghedi, I., Szakács, A., Marinel, K., Crihan, I.-M., Bernad, A., 1995. K-Ar datings of Neogene-Quaternary calc-alkaline volcanic rocks in Romania.

Pécskay, Z., Lexa, J., Szakács, A., Seghedi, I., Balogh, K., Konecny, V., Zelenka, T., Kovacs, M., Poka, T., Fulop, A., Marton, E., Panaiotu, C., Cvetkovic, V., 2006. Geochronology of Neogene magmatism in the Carpathian arc and intra-Carpathian area. Geologica Carpathica 57, 511–530.

Peltz, S., Vajdea, E., Balogh, K., Pécskay, Z., 1987. Contributions to the chronological study of the volcanic processes in the Cãlimani and Harghita Mountains (East Carpathians, Romania). Compte Rendu de Institute de Geologie e Geofisique 72, 1.

Peresson, H., Decker, K., 1997. Far-field effects of Late Miocene subduction in the Eastern Carpathians: E-W compression and inversion of structures in the Alpine-Carpathian-Pannonian region. Tectonics 16, 38–56. https://doi.org/10.1029/96TC02730

Persson, K.S., Garcia-Castellanos, D., Sokoutis, D., 2004. River transport effects on compressional belts: First results from an integrated analogue-numerical model. Journal of Geophysical Research: Solid Earth 109.

Peulvast, J.-P., Claudino Sales, V., 2005. Surfaces d'aplanissement et géodynamique. Géomorphologie : relief, processus, environnement 11, 249–274. https://doi.org/10.4000/geomorphologie.605

Popescu, S.-M., 2006. Late Miocene and early Pliocene environments in the southwestern Black Sea region from high-resolution palynology of DSDP Site 380A (Leg 42B). Palaeogeography, Palaeoclimatology, Palaeoecology 238, 64–77.

Popescu, S.-M., 2002. Repetitive changes in Early Pliocene vegetation revealed by high-resolution pollen analysis: revised cyclostratigraphy of southwestern Romania. Review of Palaeobotany and Palynology 120, 181–202.

Rădulescu, D.P., Săndulescu, M., 1973. The plate-tectonics concept and the geological structure of the Carpathians. Tectonophysics 16, 155–161. https://doi.org/10.1016/0040-1951(73)90010-3

Reiners, P.W., Ehlers, T.A., Mitchell, S.G., Montgomery, D.R., 2003. Coupled spatial variations in precipitation and long-term erosion rates across the Washington Cascades. Nature 426, 645–647. https://doi.org/10.1038/nature02111

Ricci, J., Lahitte, P., Quidelleur, X., 2015a. Construction and destruction rates of volcanoes within tropical environment: Examples from the Basse-Terre Island (Guadeloupe, Lesser Antilles). Geomorphology 228, 597–607. https://doi.org/10.1016/j.geomorph.2014.10.002

Ricci, J., Quidelleur, X., Lahitte, P., 2015b. Volcanic evolution of central Basse-Terre Island revisited on the basis of new geochronology and geomorphology data. Bulletin of Volcanology 77, 84.

1019 Ruxton, B.P., McDougall, I., 1967. Denudation rates in northeast Papua from potassium-argon dating of lavas. American
1020 Journal of Science 265, 545–561.

1021 Salvany, T., Lahitte, P., Nativel, P., Gillot, P.-Y., 2012. Geomorphic evolution of the Piton des Neiges volcano (Réunion Island,
1022 Indian Ocean): Competition between volcanic construction and erosion since 1.4Ma. Geomorphology 136, 132–147.
1023 https://doi.org/10.1016/j.geomorph.2011.06.009

1024 Samper, A., Quidelleur, X., Lahitte, P., Mollex, D., 2007. Timing of effusive volcanism and collapse events within an oceanic
1025 arc island: Basse-Terre, Guadeloupe archipelago (Lesser Antilles Arc). Earth and Planetary Science Letters 258, 175–191.
1026 https://doi.org/10.1016/j.epsl.2007.03.030

1027 Sandulescu, M., 1988. Cenozoic Tectonic History of the Carpathians: Chapter 2.

1028 Schreiber, W., Unger, E., 2006. Some specific aspects of postvolcanic relief evolution in the Harghita Mountains. (in
1029 Hungarian with English abstract). Földtani Közlöny, 136/1, 285-298.

1030 Seghedi, Downes, H., Harangi, S., Mason, P.R.D., Pécskay, Z., 2005a. Geochemical response of magmas to Neogene-
1031 Quaternary continental collision in the Carpathian-Pannonian region: A review. Tectonophysics 410, 485–499.
1032 https://doi.org/10.1016/j.tecto.2004.09.015

1033 Seghedi, I., 1995. The Călimani-Gurghiu-Harghita volcanic chain, East Carpathians, Romania: volcanological features.

1034 Seghedi, I., Balintoni, I., Szakács, A., 1998. Interplay of tectonics and neogene post-collisional magmatism in the
1035 intracarpathian region. Lithos 45, 483–497. https://doi.org/10.1016/S0024-4937(98)00046-2

1036 Seghedi, I., Downes, H., Vaselli, O., Szakács, A., Balogh, K., Pécskay, Z., 2004a. Post-collisional Tertiary–Quaternary mafic
1037 alkalic magmatism in the Carpathian–Pannonian region: a review. Tectonophysics 393, 43–62.
1038 https://doi.org/10.1016/j.tecto.2004.07.051

1039 Seghedi, I., Maţenco, L., Downes, H., Mason, P.R.D., Szakács, A., Pécskay, Z., 2011. Tectonic significance of changes in post-
1040 subduction Pliocene–Quaternary magmatism in the south east part of the Carpathian–Pannonian Region. Tectonophysics
1041 502, 146–157. https://doi.org/10.1016/j.tecto.2009.12.003

1042 Seghedi, I., Mirea, V., Popa, R.-G., Szakács, A., 2019. Tectono-magmatic characteristics of post-collisional magmatism: Case
1043 study East Carpathians, Călimani-Gurghiu-Harghita volcanic range. Physics of the Earth and Planetary Interiors 293, 106270.
1044 https://doi.org/10.1016/j.pepi.2019.106270

1045 Seghedi, I., Szakács, A., Snelling, N.J., Pécskay, Z., 2004b. Evolution of the Neogene Gurghiu Mountains volcanic range
1046 (Eastern Carpathians, Romania), based on K-Ar geochronology. Geologica Carpathica 55, 325–332.

1047 Seghedi, Szakács, A., Pécskay, Z., Mason, P.R.D., 2005b. Eruptive history and age of magmatic processes in the Cãlimani
1048 volcanic structure (Romania) 10.

1049 Simon-Coinçon, R., 1989. Le rôle des paléoaltérations et des paléoformes dans les socles : l'exemple du Rouergue (Massif
1050 Central français). Centre de géologie générale et minière.

1051 Slingerland, R., Furlong, K.P., 1989. Geodynamic and geomorphic evolution of the Permo-Triassic Appalachian Mountains.
1052 Geomorphology 2, 23–37.

1053 Smith, S.G., Wegmann, K.W., Ancuta, L.D., Gosse, J.C., Hopkins, C.E., 2016. Paleotopography and erosion rates in the central
1054 Hangay Dome, Mongolia: Landscape evolution since the mid-Miocene. Journal of Asian Earth Sciences 125, 37–57.
1055 https://doi.org/10.1016/j.jseaes.2016.05.013

1056 Sturt, B.A., Dalland, A., Mitchell, J.L., 1979. The age of the sub Mid-Jurassic tropical weathering profile of Andoya, northern
1057 Norway, and the implications for the late Palaeozoic palaeography in the North Atlantic region. Geologische Rundschau 68,
1058 523–542.

1059 Suc, J.-P., 1984. Origin and evolution of the Mediterranean vegetation and climate in Europe. Nature 307, 429.

1060 Szabó, C., Harangi, S., Csontos, L., 1992. Review of Neogene and Quaternary volcanism of the Carpathian-Pannonian region
1061 14.

1062 Szakács, A., Ioane, D., Seghedi, I., Rogobete, M., Pécskay, Z., 1997. Rates of migration of volcanic activity and magma out
1063 put along the Calimani-Gurghiu-Harghita volcanic range, East Carpathians, Romania. Przegląd Geologiczny 45, 1106.

1064 Szakács, A., Krézsek, C., 2006. Volcano–basement interaction in the Eastern Carpathians: Explaining unusual tectonic
1065 features in the Eastern Transylvanian Basin, Romania. Journal of Volcanology and Geothermal Research 158, 6–20.
1066 https://doi.org/10.1016/j.jvolgeores.2006.04.012

1067 Szakács, A., Seghedi, I., 2000. Large volume volcanic debris avalanche in the East Carpathians, Romania. Volcaniclastic rocks,
1068 from magmas to sediments, Gordon Breach Science Publishers, Amsterdam, The Netherlands 131–151.

1069 Szakács, A., Seghedi, I., 1996. Volcaniclastic sequences around andesitic stratovolcanoes, East Carpathians, Romania.
1070 Romanian Journal of Petrology 77, 1–55.

Szakács, A., Seghedi, I., 1995. The Călimani-Gurghiu-Harghita volcanic chain. East Carpathians.

Szakács, A., Seghedi, I., Pécskay, Z., 1993. Peculiarities of South Harghita Mts as a Terminal Segment of the Carpathian Neogene to Quaternary Volcanic Chain. Editura Academiei Române.

Székely, B., Karátson, D., 2004. DEM-based morphometry as a tool for reconstructing primary volcanic landforms: examples from the Börzsöny Mountains, Hungary. Geomorphology 63, 25–37. https://doi.org/10.1016/j.geomorph.2004.03.008

Tari, G., Dövényi, P., Dunkl, I., Horváth, F., Lenkey, L., Stefanescu, M., Szafián, P., Tóth, T., 1999. Lithospheric structure of the Pannonian basin derived from seismic, gravity and geothermal data. Geological Society, London, Special Publications 156, 215–250.

Thouret, J.-C., 1999. Volcanic geomorphology—an overview. Earth-Science Reviews 47, 95–131. https://doi.org/10.1016/S0012-8252(99)00014-8

Thouret, J.-C., Oehler, J.-F., Gupta, A., Solikhin, A., Procter, J.N., 2014. Erosion and aggradation on persistently active volcanoes—a case study from Semeru Volcano, Indonesia. Bulletin of Volcanology 76, 857.

Traverse, A., 1978. Palynological analysis of DSDP Leg 42B (1975) cores from the Black Sea. Initial Report DSDP 42, 993–1016.

Tucker, G.E., Hancock, G.R., 2010. Modelling landscape evolution. Earth Surface Processes and Landforms 35, 28–50.

Vidal, V., Bonneville, A., 2004. Variations of the Hawaiian hot spot activity revealed by variations in the magma production rate. https://doi.org/10.1029/2003JB002559

Wadge, G., 1984. Comparison of volcanic production rates and subduction rates in the Lesser Antilles and Central America. Geology 12, 555–558.

Wadge, G., 1982. Steady state volcanism: Evidence from eruption histories of polygenetic volcanoes. Journal of Geophysical Research: Solid Earth 87, 4035–4049. https://doi.org/10.1029/JB087iB05p04035

White, S.M., Crisp, J.A., Spera, F.J., 2006. Long-term volumetric eruption rates and magma budgets. Geochemistry, Geophysics, Geosystems 7. https://doi.org/10.1029/2005GC001002

Wooller, L., van Wyk de Vries, B., Murray, J.B., Rymer, H., Meyer, S., 2004. Volcano spreading controlled by dipping substrata. Geology 32, 573. https://doi.org/10.1130/G20472.1

1096 Wright, R., Garbeil, H., Baloga, S.M., Mouginis-Mark, P.J., 2006. An assessment of shuttle radar topography mission digital
1097 elevation data for studies of volcano morphology. Remote Sensing of Environment 105, 41–53.

1098 Yokoyama, R., Shirasawa, M., Pike, R.J., 2002. Visualizing Topography by Openness: A New Application of Image Processing
1099 to Digital Elevation Models.

1100 Zernack, A.V., Cronin, S.J., Neall, V.E., Procter, J.N., 2011. A medial to distal volcaniclastic record of an andesite
1101 stratovolcano: detailed stratigraphy of the ring-plain succession of south-west Taranaki, New Zealand. International Journal
1102 of Earth Sciences 100, 1937–1966.

Figure Captions

Fig. 1: Geological setting of the studied area (East Carpathian Volcanic Range). Each volcano is labelled as following (Romanian names, Hungarian ones can be found in Table 1): Călimani sector (surrounded by red outline): 01 – Central Călimani including Rusca-Tihu cones Lucaciul, Tămăul and Călimani caldera; 02 – Moldovanul. Gurghiu sector (green outline): 03 - Jirca; 04 – Fâncel-Lăpuşna, including cones Fâncel (04a) and Obarsia (04b); 05 –Bacta; 06 – Seaca-Tătarca; 07 – Ciumani; 08 – Borzont; 09 – Şumuleu including cone Şumuleu (09a) and Vf. Ascuţit (09b). North Harghita sector (blue outline): 10 – Ostoroş; 11 – Ivo-Cocoizaş; 12 – Râchitis; 13a – Vârghiş and 13b – Szeles Vésze cone. South Harghita sector (yellow outline): 14 – Luci-Lazu (14a and 14b); 15 – Cucu; 16 – Pilişca; 17 –Ciomadul lavas domes. Inset: Regional topographic sketch map of Carpathian orogen.

Fig. 2 : A) Constraining points (CPs) of each single volcanic edifice. New unspiked K/Ar ages (in Ma): A) Călimani. B) Seaca-Tătarca volcano. C) Vârghiş volcano. D) Pilişca volcano.

Fig. 3 : Modelling of the best fitting surface with all relevant parameters, example of Seaca-Tătarca volcano: A) Elevation versus distance to centre diagram, green dots project the whole volcano surface, purple dots are CPs and black dots are the best model profile. B) Projection of mean (orange), max (yellow) and min (grey) elevation of the whole volcano surface, after a summarization by a 100m-long window. Note how the best model profile (black dot) fit well with the upper surface (yellow dots). Average altitude loss (blue dots) computed as the difference between the best model profile and the mean elevation profile. C) Perspective view of the best modelled surface: purple dots are the CPs extracted from the

DEM (coloured surface). Coloured dots show the best modelled surface. Black sticks highlight the loss of elevation (i.e. the intensity of erosion).

Fig. 4 : Modelled paleo-volcanic surfaces (as they would be directly after the cessation of volcanism, i.e. before erosion effect): A) North (red colours) - South (yellow colours) cross-section and perspective views of the whole reconstructed CGH range. B), C), D) zoomed representation of Gurghiu, North Harghita and South Harghita sectors, respectively. Numbers refer as the same labels as in Fig. 1 and Table 2. Cream coloured surface is the pre-volcanic basement surface (PVBS).

Fig. 5 : **A**) Correlation between total constructed volume with volcano area (uncertainties displayed at 1σ-level): Green line and box parameters: power-law fitting function obtained with consideration of all volcanoes. Black line and box parameters: fitting without consideration of Făncel-Lâpuşna volcano (green dot). Inset: height and volume of CGH volcanoes plotted on the height versus volume diagram of Grosse et al. (2009) with fitting power-law function. **B**) Correlation of eroded volume with constructed volume of each CGH volcano: circle diameters with respect to degree of denudation values (expressed in %). Colour of symbols, line and parameters box refer to volcano ages: older (red), intermediate (green) and youngest (yellow) volcanoes. Black line and parameters box represent the V_E-V_C correlations for all volcanoes whereas colour lines show fitting for the corresponding periods. Black arrow explained in text.

Fig. 6 : Correlation between degree of denudation of each volcano of the range with **A)** the height. **B**) the latitude. Colours symbols with respect to belonging segment (yellow: South Harghita, blue: North Harghita, green: Gurghiu, red; Călimani).

Fig. 7 : Relative uncertainty of constructed volume versus average height diagram with best fitting function. Circle diameter proportional to volcano volume.

Fig. 8 : Model of growth of Seaca-Tătarca volcano through time: **A)** Projection in elevation versus distance to centre of the whole Seaca-Tătarca volcano surface (green dots) with projection of the dated samples (white dots). Blue line displays the chronological model of growth based on the modelled uppermost volcanic surface. Note how the blue lines regularly spaced every each 10% of volume become closer upward. **B)** Proportions of constructed of Seaca-Tătarca volcano versus time diagram. White dots: growth proportion associated to each dated sample deduced from Fig. 8A, red dots represent interpolation of 0 and 100% of construction (i.e. begin and end of the activity).

Fig. 9 : All available ages of CGH volcanic range projected along a N-S profile (Y-axis is the UTM coordinates of samples). Colours symbols as in Fig. 5 except grey symbols plotting newly dated samples. Coloured outlines display the spatio-temporal range of volcanic activity. Heavy lines show either the expansion (Gurghiu case, using only heavily outlined green symbols) or migration (N. and S. Harghita cases, using all their respective ages) through time (details in the text), with quantification in the coloured rectangles. Black double arrows highlight the synchronism in sectors.

Fig. 10 : Cumulative volume and magma output rates through time (A), correlated to the main Tertiary tectonic events affecting the East Carpathian range (displayed as cartoons B, C and D). **A)** Individual variation of volcanic output through time (coloured lines). Cumulative erupted volume (dashed line and left axis) and global growth rate (plain line and right axis) variations through time over the whole CGH range. Inset displays Fig. 10 to highlight volume – space correlations. **B)** Oceanic crust subduction occurring during the Early–Mid-Miocene

convergence episode. **C)** Thinned continental crust subduction and collisional features in the overriding plate. **D)** Slab detachment of the dense oceanic lithosphere from buoyant continental lithosphere and upwelling of the hot asthenospheric mantle into the gap to be juxtaposed against the base of the mechanical lithosphere.

Fig. 11 : Volumes versus lifespan in a log-log diagram. Trends of both group (red and blue diagonal lines) as well as grey dashed lines represent constant rates of magma output. Background of the figure displaying various volcanic contexts around the world from White et al. (2006).

Fig. 12 : Graph of dismantling parameters versus time. Black and grey circles (left axis) are the computed degree of denudation values of each volcano (i.e. averaged along its whole erosion history), fitted by the reverse exponential curve (with parameters in the blue box). Grey circles are values from the dozen domes of the Ciomadul volcanic complex (Karátson et al., 2019; Lahitte et al., 2019; details in S.M.), black dots are D_{Den} values from this work (all other CGH volcanoes). Orange and red circles are the cumulative averaged erosion rate of each volcano (right axis) and fitted by the red quadratic curve. Contrarily to red/orange circles that show average-integrated erosion rates, large diamonds (right axis) represent the erosion rates computed for specific periods when specific climatic context (summarized on top of the figure) occurred: red diamond for erosion regime occurring during 10.8 - 6.9 Ma; green diamond: 8.7 - 5.5 Ma; blue diamond: 7.0-4.6 Ma; yellow diamond: Quaternary.

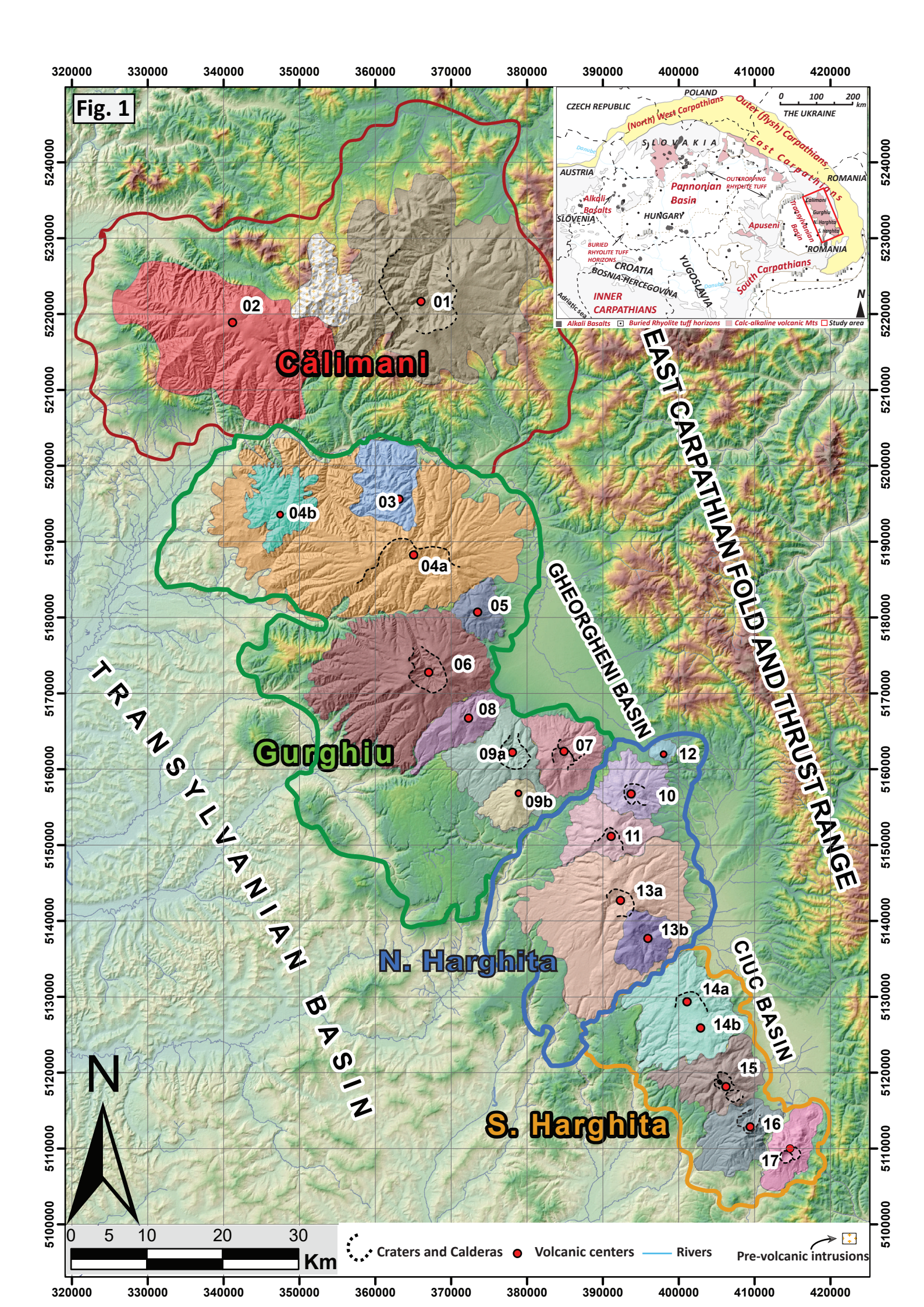
Fig. 1
Călimani
Gurghiu
N. Harghita
S. Harghita
TRANSYLVANIAN BASIN
GHEORGHENI BASIN
EAST CARPATHIAN FOLD AND THRUST RANGE
CIUC BASIN
01
02
03
04a
04b
05
06
07
08
09a
09b
10
11
12
13a
13b
14a
14b
15
16
17
POLAND
CZECH REPUBLIC
THE UKRAINE
SLOVAKIA
AUSTRIA
HUNGARY
SLOVENIA
CROATIA
BOSNIA-HERCEGOVINA
YUGOSLAVIA
ROMANIA
(North) West Carpathians
Outer (flysh) Carpathians
East Carpathians
Pannonian Basin
Alkali Basalts
OUTCROPPING RHYOLITE TUFF
BURIED RHYOLITE TUFF HORIZONS
Transylvanian Basin
Apuseni
South Carpathians
INNER CARPATHIANS
Danube
Adriatic sea
Alkali Basalts
Buried Rhyolite tuff horizons
Calc-alkaline volcanic Mts
Study area
0 5 10 20 30 Km
Craters and Calderas
Volcanic centers
Rivers
Pre-volcanic intrusions

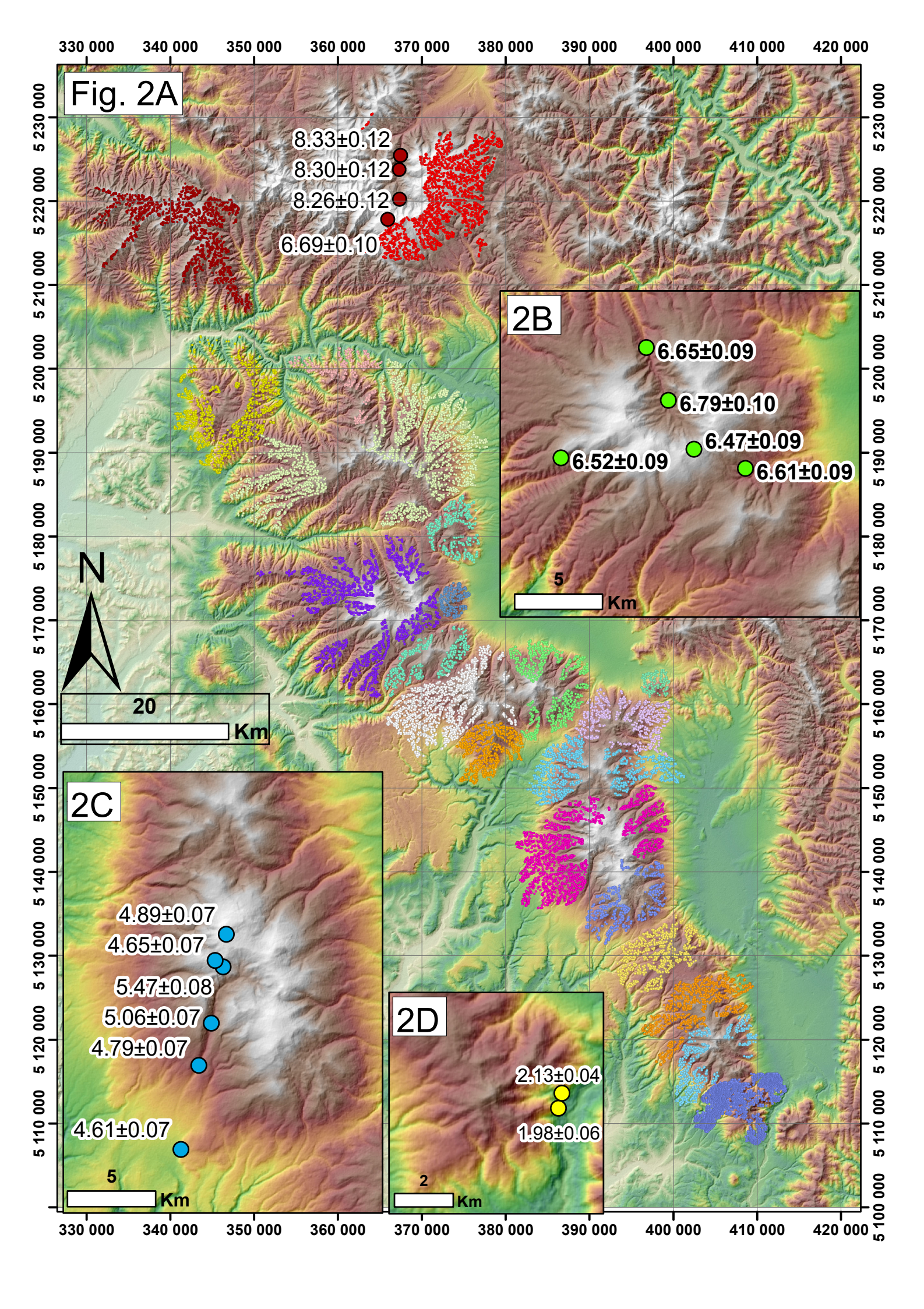
Fig. 2A
8.33±0.12
8.30±0.12
8.26±0.12
6.69±0.10
2B
6.65±0.09
6.79±0.10
6.47±0.09
6.52±0.09
6.61±0.09
5
Km
N
20
Km
2C
4.89±0.07
4.65±0.07
5.47±0.08
5.06±0.07
4.79±0.07
4.61±0.07
5
Km
2D
2.13±0.04
1.98±0.06
2
Km
330 000
340 000
350 000
360 000
370 000
380 000
390 000
400 000
410 000
420 000
5 230 000
5 220 000
5 210 000
5 200 000
5 190 000
5 180 000
5 170 000
5 160 000
5 150 000
5 140 000
5 130 000
5 120 000
5 110 000
5 100 000

Fig. 3

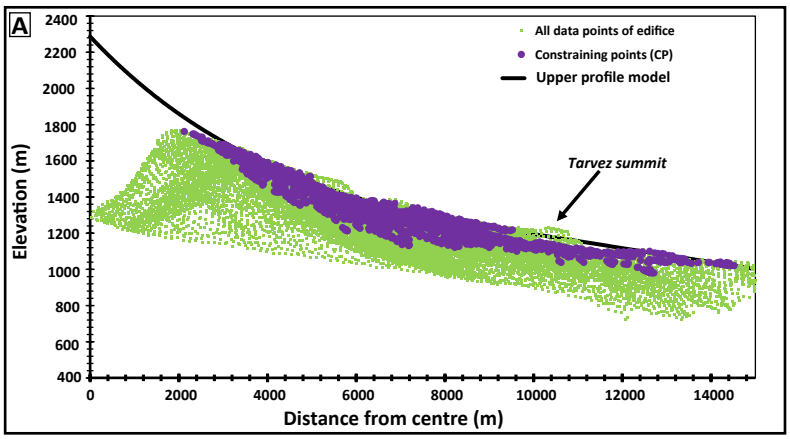
A
All data points of edifice
Constraining points (CP)
Upper profile model
Tarvez summit
Elevation (m)
Distance from centre (m)

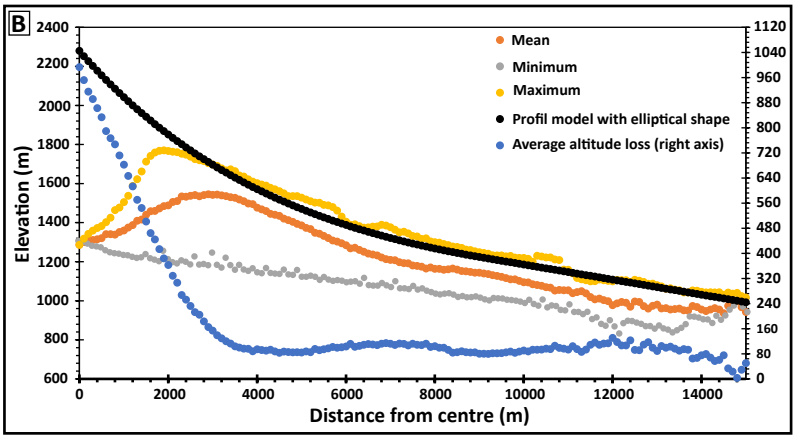
B
Mean
Minimum
Maximum
Profil model with elliptical shape
Average altitude loss (right axis)
Elevation (m)
Distance from centre (m)

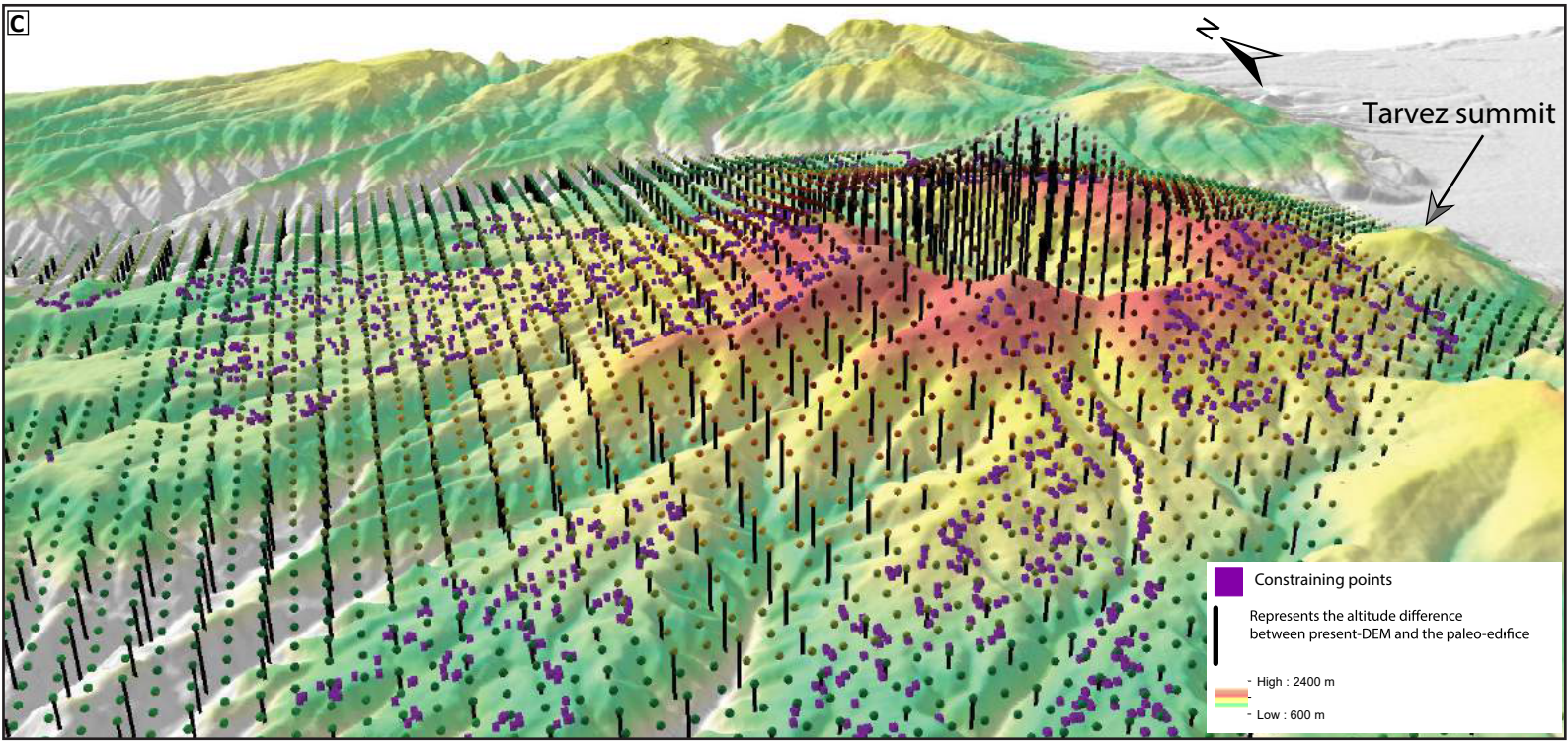
C
N
Tarvez summit
Constraining points
Represents the altitude difference between present-DEM and the paleo-edifice
High : 2400 m
Low : 600 m

Fig. 4

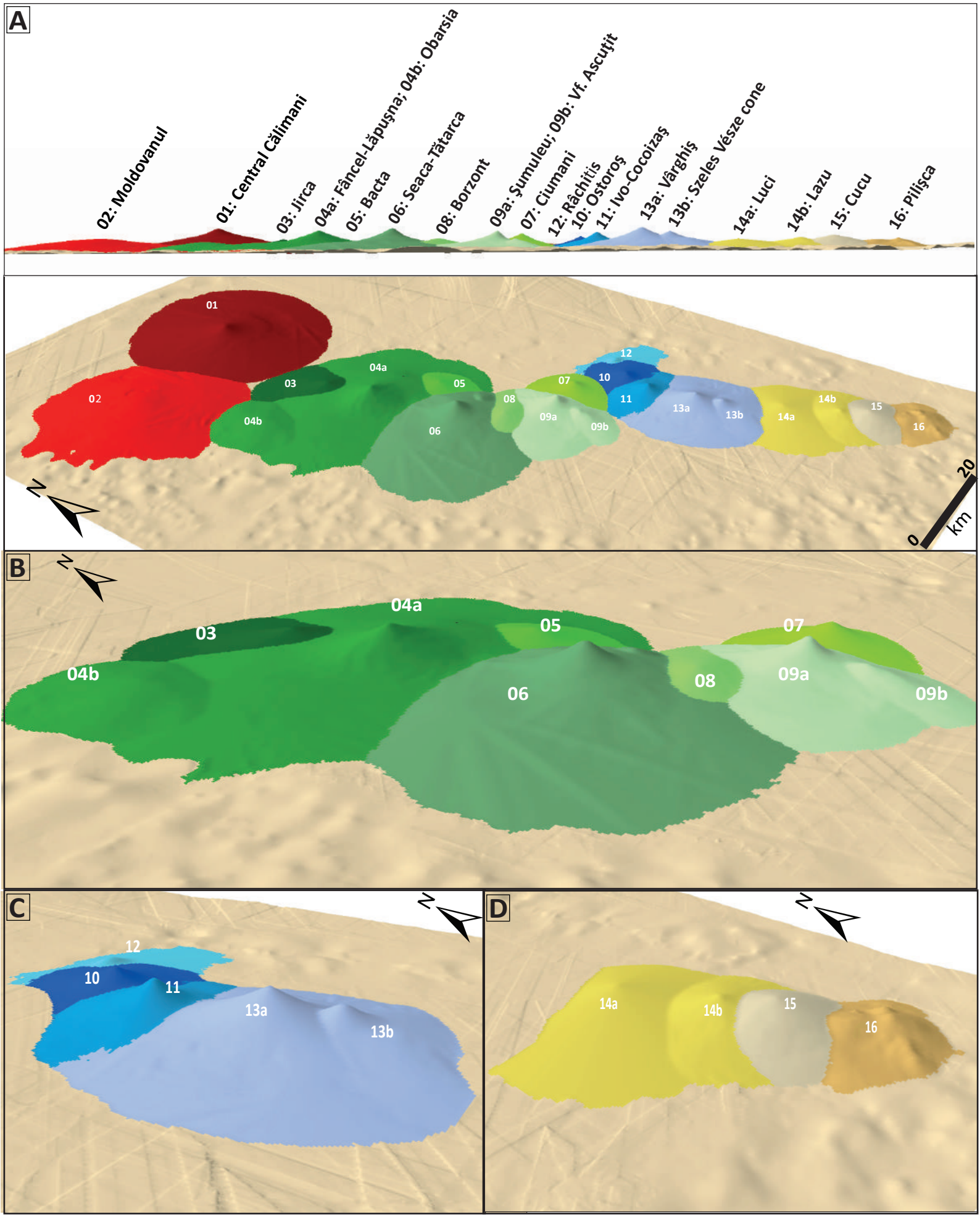
A
02: Moldovanul
01: Central Călimani
03: Jirca
04a: Fâncel-Lăpuşna; 04b: Obarsia
05: Bacta
06: Seaca-Tătarca
08: Borzont
09a: Şumuleu; 09b: Vf. Ascuţit
07: Ciumani
12: Râchiţiş
10: Ostoroş
11: Ivo-Cocoizaş
13a: Vârghiş
13b: Szeles Vésze cone
14a: Luci
14b: Lazu
15: Cucu
16: Pilişca
01
02
03
04a
04b
05
06
07
08
09a
09b
10
11
12
13a
13b
14a
14b
15
16
N
0
20
km
B
N
04a
03
05
07
04b
06
08
09a
09b
C
N
12
10
11
13a
13b
D
N
14a
14b
15
16

Fig. 5

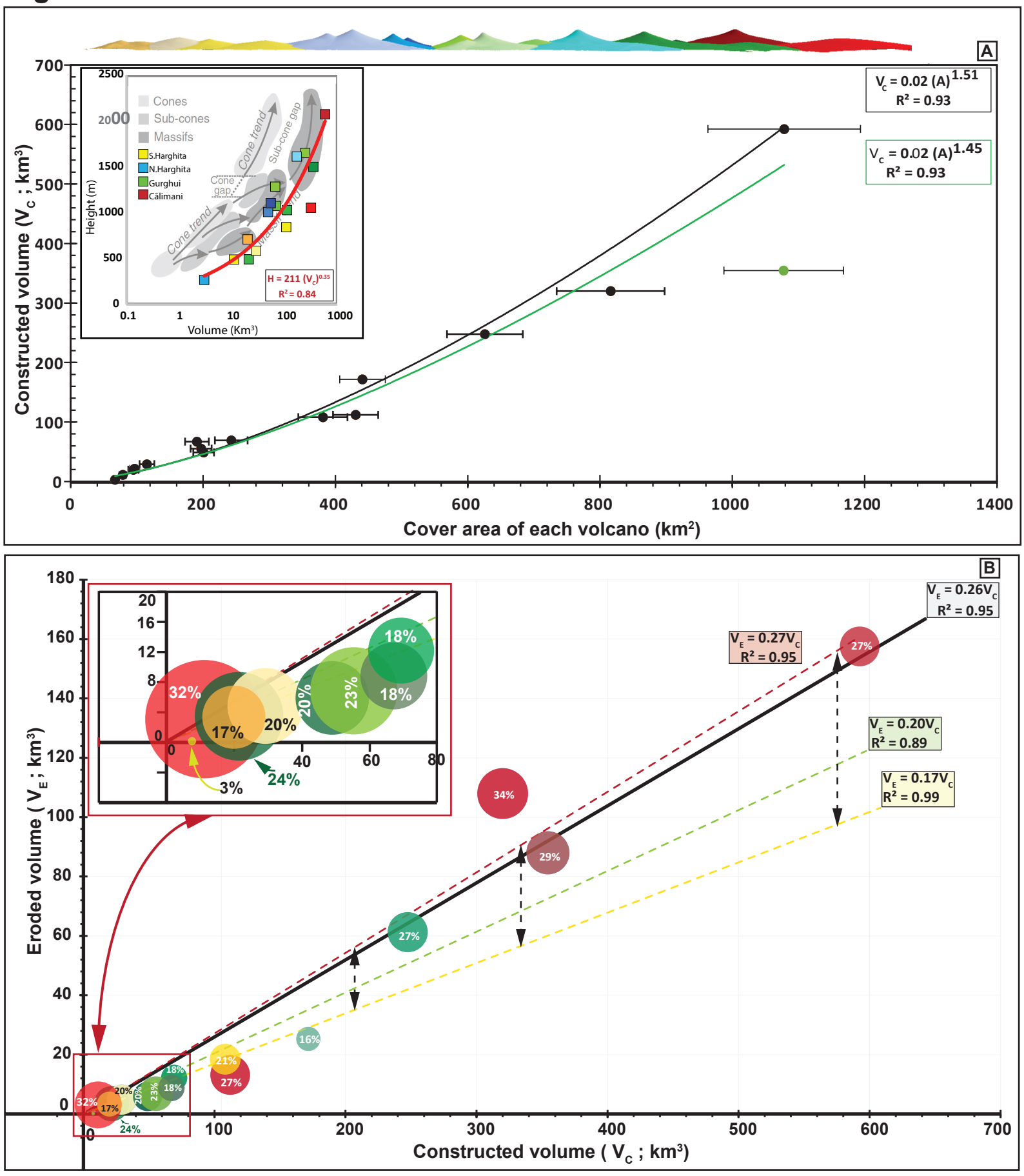
A
Constructed volume (V_C ; km³)
Cover area of each volcano (km²)
$V_C = 0.02 (A)^{1.51}$
$R^2 = 0.93$
$V_C = 0.02 (A)^{1.45}$
$R^2 = 0.93$
Cones
Sub-cones
Massifs
S.Harghita
N.Harghita
Gurghui
Călimani
Cone trend
Sub-cone gap
Cone gap
Massif trend
Height (m)
Volume (Km³)
$H = 211 (V_C)^{0.35}$
$R^2 = 0.84$
B
Eroded volume (V_E ; km³)
Constructed volume (V_C ; km³)
$V_E = 0.26V_C$
$R^2 = 0.95$
$V_E = 0.27V_C$
$R^2 = 0.95$
$V_E = 0.20V_C$
$R^2 = 0.89$
$V_E = 0.17V_C$
$R^2 = 0.99$
32%
17%
20%
3%
24%
20%
23%
18%
18%
34%
29%
27%
27%
16%
21%
27%

Fig. 6

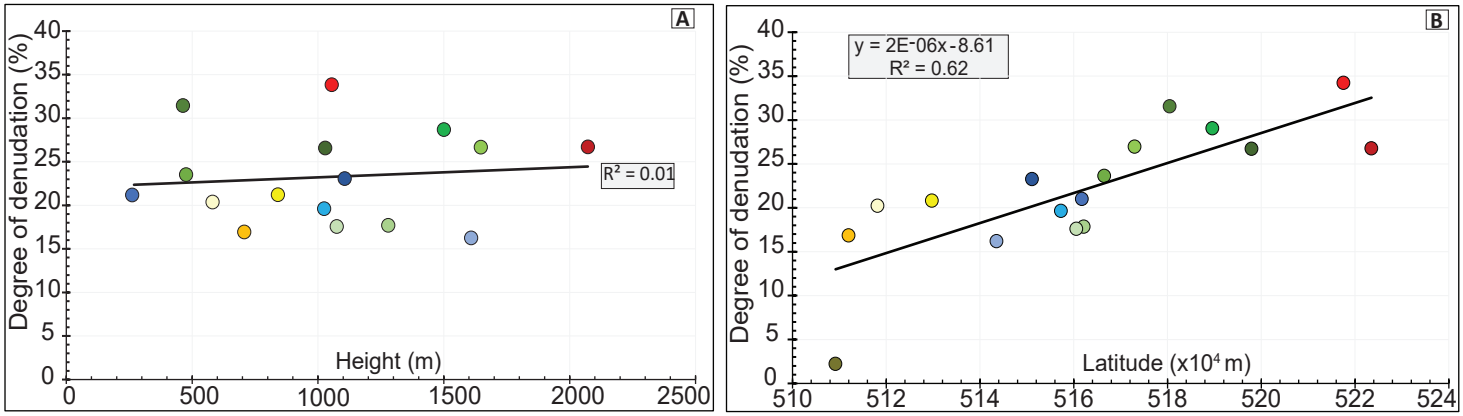
A
Degree of denudation (%)
Height (m)
R² = 0.01
0
5
10
15
20
25
30
35
40
0
500
1000
1500
2000
2500
B
y = 2E-06x - 8.61
R² = 0.62
Degree of denudation (%)
Latitude (x10⁴ m)
510
512
514
516
518
520
522
524

Fig. 7

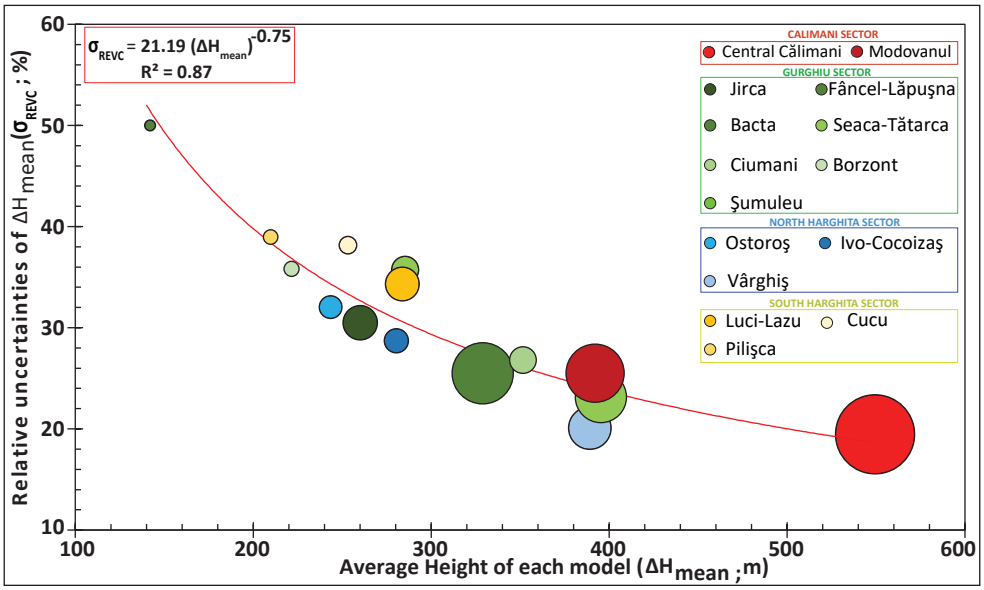
σREVC = 21.19 (ΔHmean)-0.75
R² = 0.87
CALIMANI SECTOR
Central Călimani
Modovanul
GURGHIU SECTOR
Jirca
Fâncel-Lăpuşna
Bacta
Seaca-Tătarca
Ciumani
Borzont
Şumuleu
NORTH HARGHITA SECTOR
Ostoroş
Ivo-Cocoizaş
Vârghiş
SOUTH HARGHITA SECTOR
Luci-Lazu
Cucu
Pilişca
Relative uncertainties of ΔH mean(σREVC ; %)
Average Height of each model (ΔHmean ;m)
10
20
30
40
50
60
100
200
300
400
500
600

Fig. 8

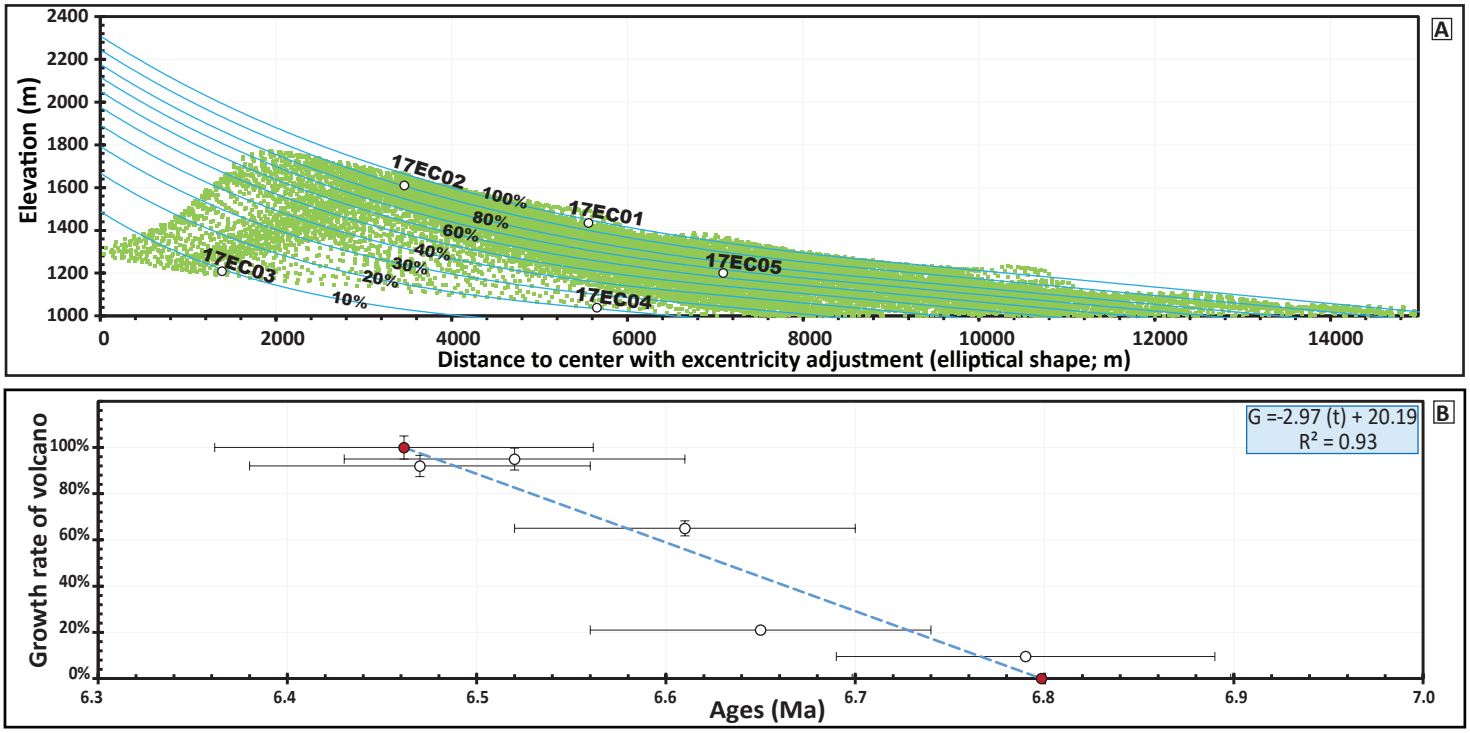
A
Elevation (m)
2400
2200
2000
1800
1600
1400
1200
1000
0
2000
4000
6000
8000
10000
12000
14000
Distance to center with excentricity adjustment (elliptical shape; m)
17EC02
17EC01
17EC05
17EC04
17EC03
100%
80%
60%
40%
30%
20%
10%

B
G =-2.97 (t) + 20.19
R² = 0.93
Growth rate of volcano
100%
80%
60%
40%
20%
0%
6.3
6.4
6.5
6.6
6.7
6.8
6.9
7.0
Ages (Ma)

Fig. 9

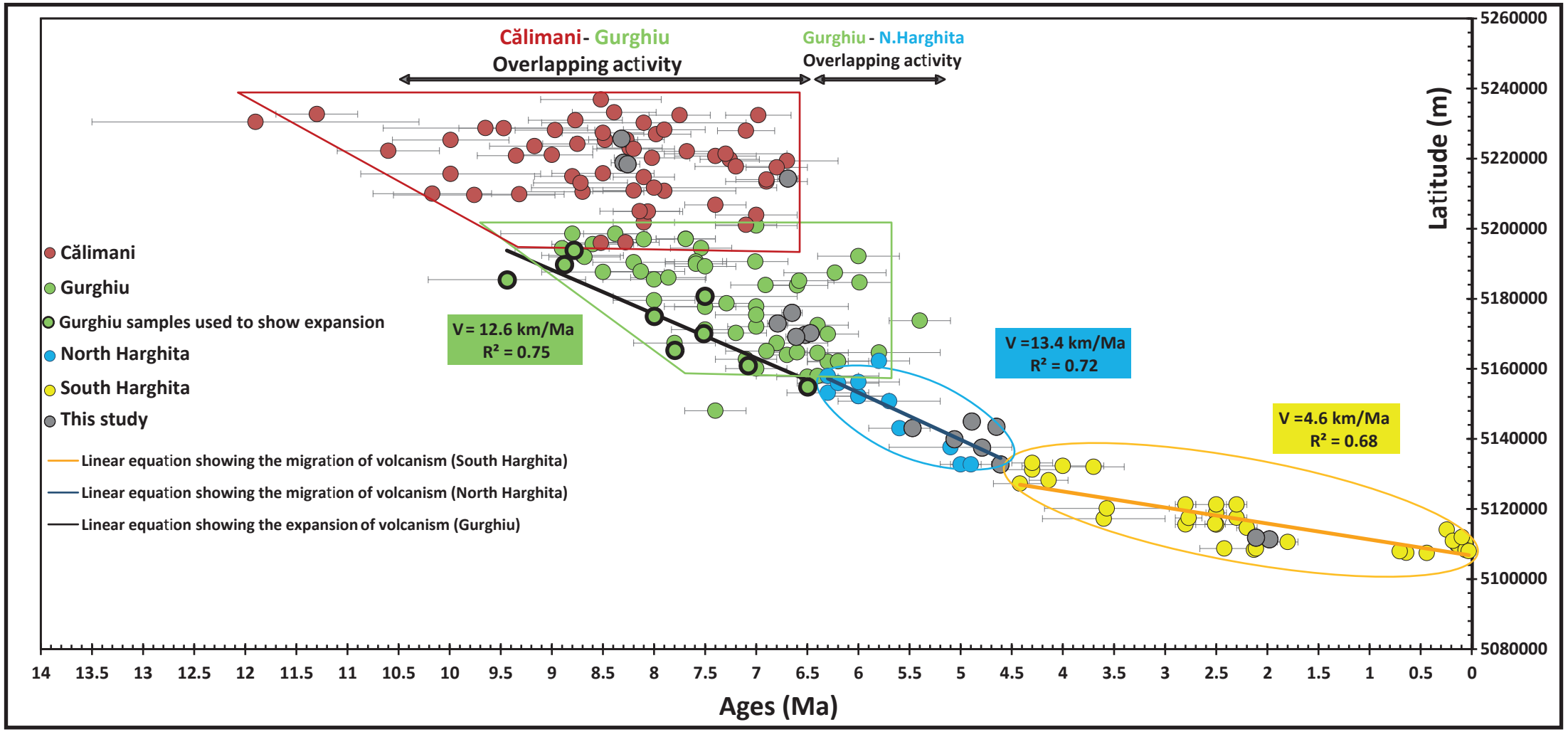
Călimani- Gurghiu
Overlapping activity
Gurghiu - N.Harghita
Overlapping activity
Călimani
Gurghiu
Gurghiu samples used to show expansion
North Harghita
South Harghita
This study
Linear equation showing the migration of volcanism (South Harghita)
Linear equation showing the migration of volcanism (North Harghita)
Linear equation showing the expansion of volcanism (Gurghiu)
V= 12.6 km/Ma
R² = 0.75
V =13.4 km/Ma
R² = 0.72
V =4.6 km/Ma
R² = 0.68
Latitude (m)
5260000
5240000
5220000
5200000
5180000
5160000
5140000
5120000
5100000
5080000
14
13.5
13
12.5
12
11.5
11
10.5
10
9.5
9
8.5
8
7.5
7
6.5
6
5.5
5
4.5
4
3.5
3
2.5
2
1.5
1
0.5
0
Ages (Ma)

Fig.10

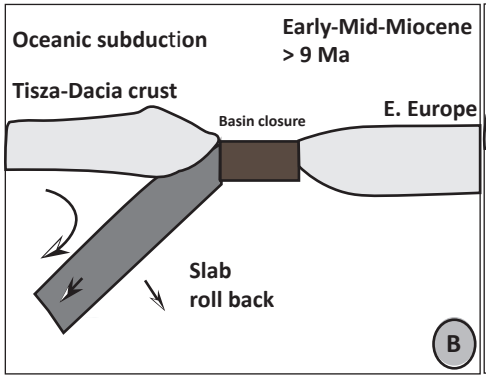
Oceanic subduction
Early-Mid-Miocene
> 9 Ma
Tisza-Dacia crust
Basin closure
E. Europe
Slab
roll back
B

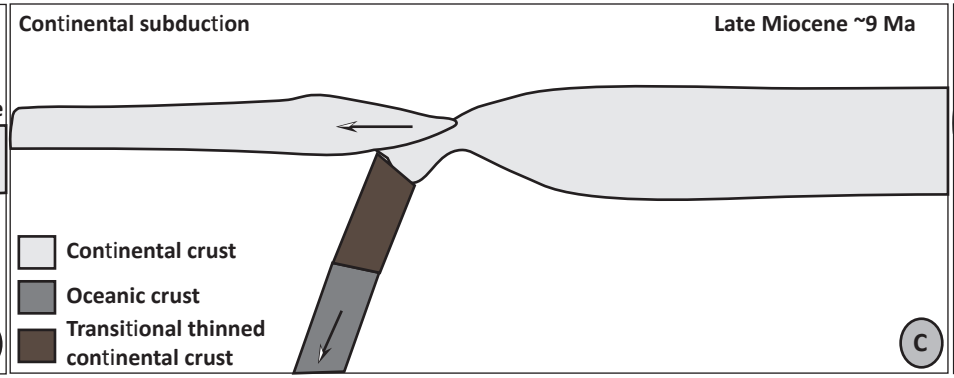
Continental subduction
Late Miocene ~9 Ma
Continental crust
Oceanic crust
Transitional thinned
continental crust
C

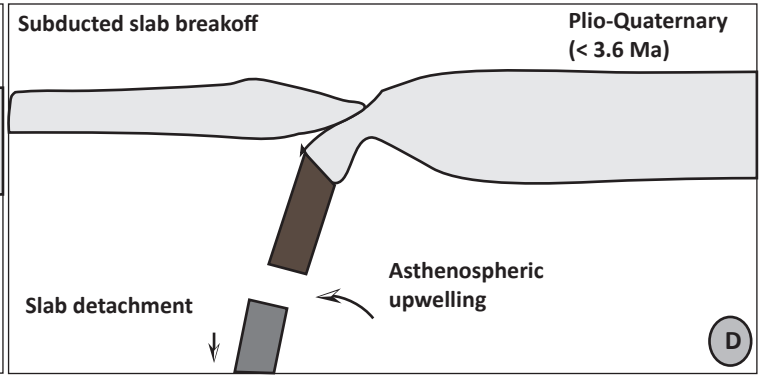
Subducted slab breakoff
Plio-Quaternary
(< 3.6 Ma)
Slab detachment
Asthenospheric
upwelling
D

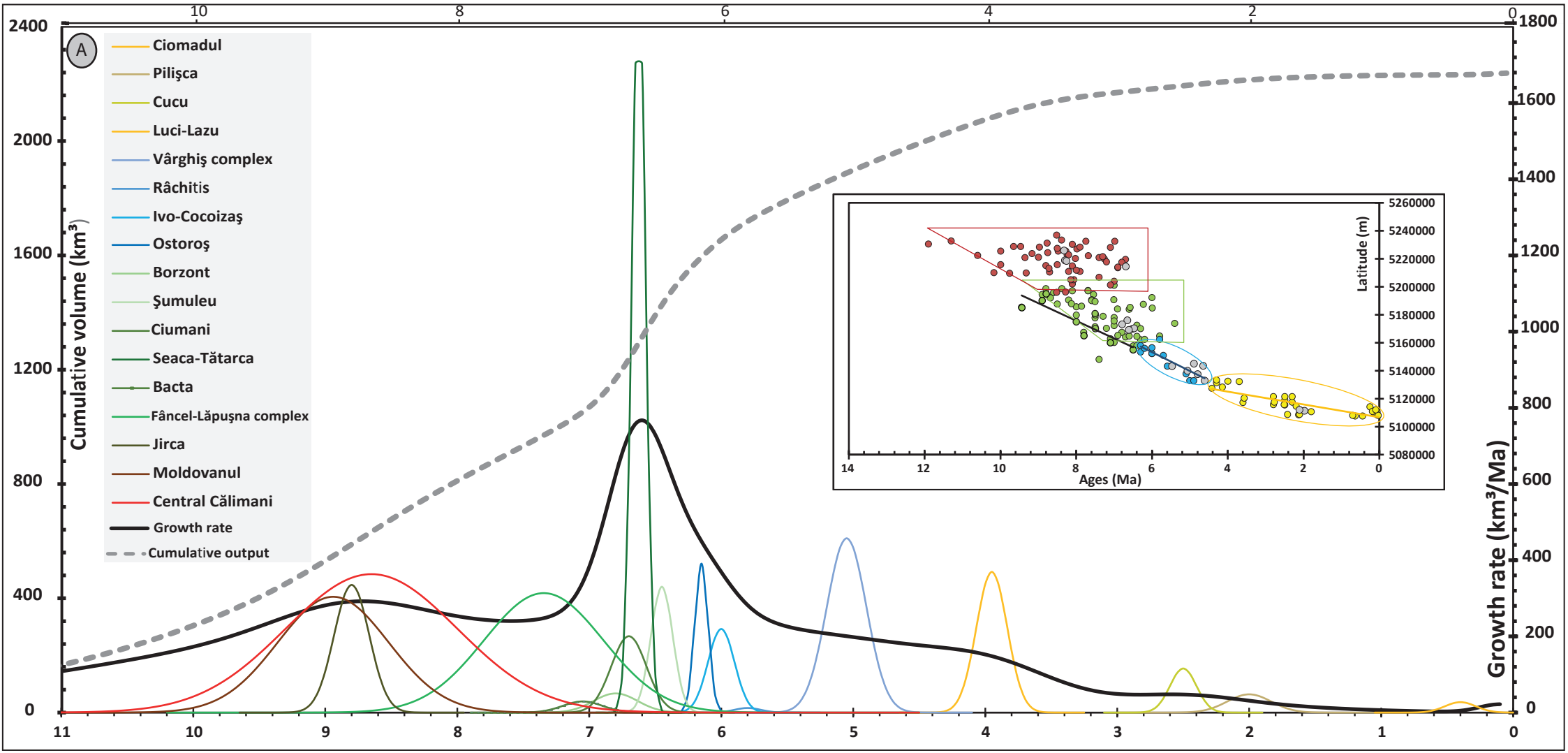
A
Ciomadul
Pilişca
Cucu
Luci-Lazu
Vârghiş complex
Râchitis
Ivo-Cocoizaş
Ostoroş
Borzont
Şumuleu
Ciumani
Seaca-Tătarca
Bacta
Fâncel-Lăpuşna complex
Jirca
Moldovanul
Central Călimani
Growth rate
Cumulative output
Cumulative volume (km³)
Growth rate (km³/Ma)
Duration (Ma)
Latitude (m)
Ages (Ma)

Fig. 11

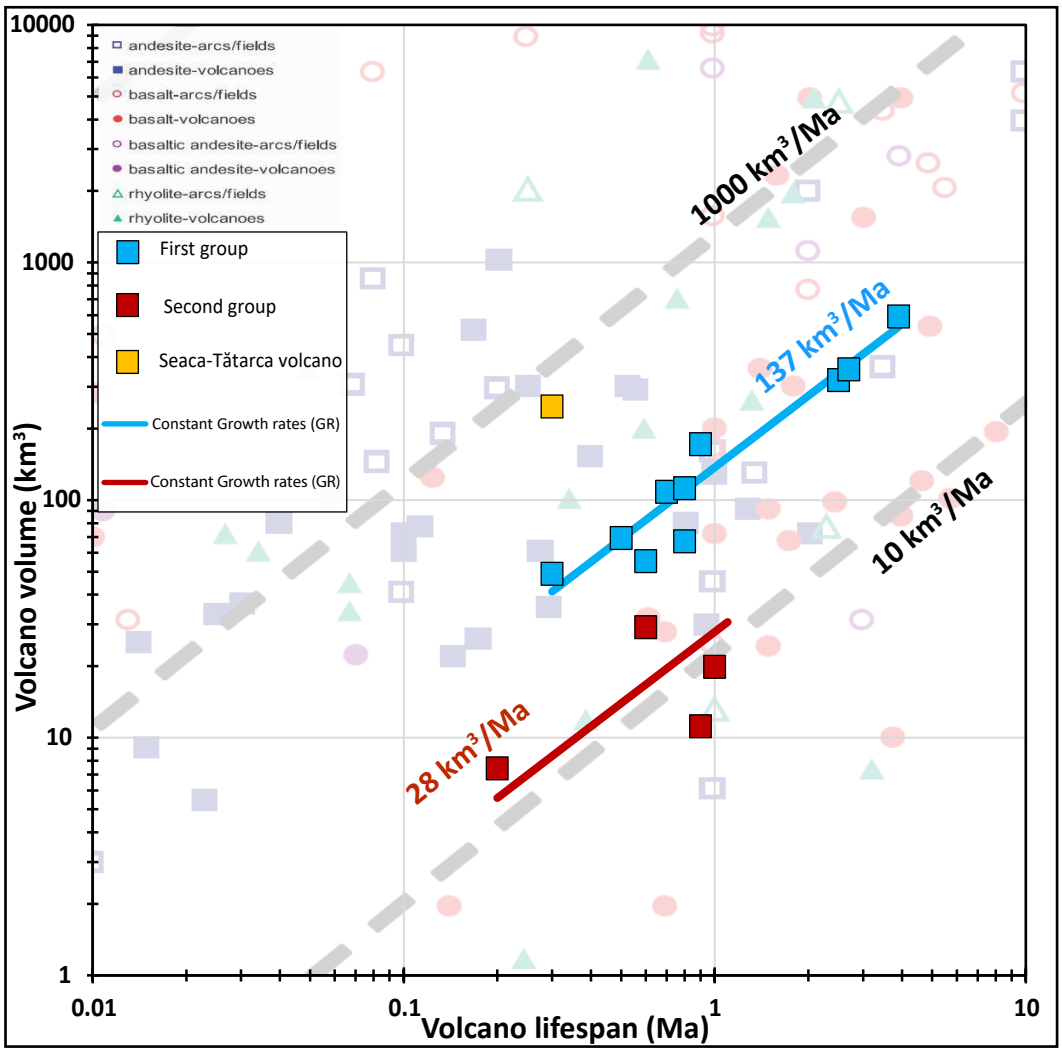
andesite-arcs/fields
andesite-volcanoes
basalt-arcs/fields
basalt-volcanoes
basaltic andesite-arcs/fields
basaltic andesite-volcanoes
rhyolite-arcs/fields
rhyolite-volcanoes
First group
Second group
Seaca-Tătarca volcano
Constant Growth rates (GR)
Constant Growth rates (GR)
1000 km³/Ma
137 km³/Ma
10 km³/Ma
28 km³/Ma
Volcano volume (km³)
Volcano lifespan (Ma)
10000
1000
100
10
1
0.01
0.1
1
10

Fig. 12

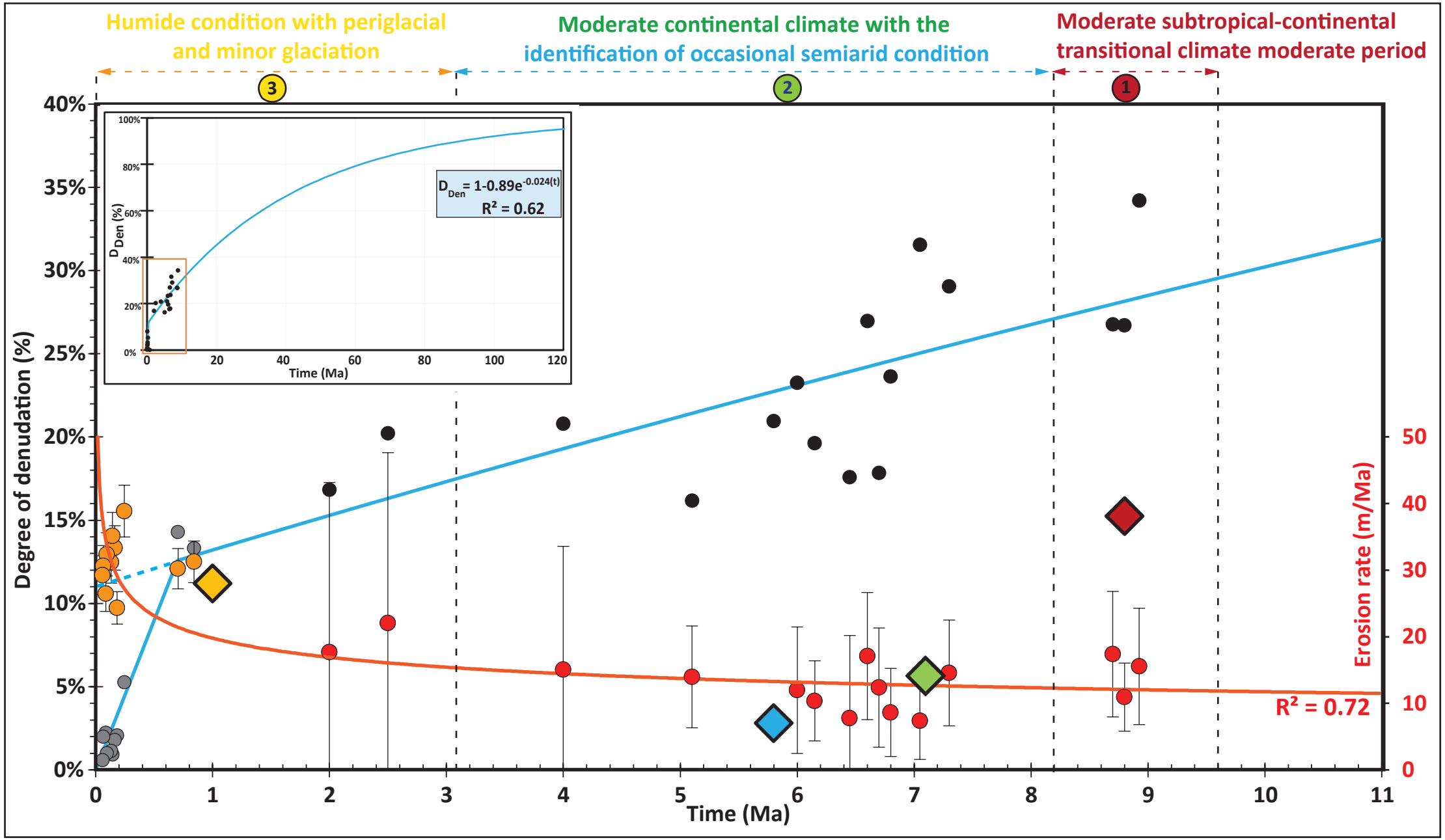
Humide condition with periglacial and minor glaciation
Moderate continental climate with the identification of occasional semiarid condition
Moderate subtropical-continental transitional climate moderate period
3
2
1
Degree of denudation (%)
Erosion rate (m/Ma)
Time (Ma)
R² = 0.72
D_Den = 1-0.89e^-0.024(t)
R² = 0.62
D_Den (%)
Time (Ma)

Tables

Table 1. New K-Ar dating results (details of measurement in S.M).

Sample code	Rock type	K%	Mean age ± 1σ (Ma)	
17EC14	Dacite	2.730	1.98±0.06	Pilișca
17EC15	Dacite	2.841	2.11±0.04	
17EC11	Pyr. andesite	1.503	4.61±0.07	Vârghiș
17EC09	Pyr. andesite	1.551	4.65±0.07	
17EC06	Pyr. andesite	1.932	4.79±0.07	
17EC10	Pyr. andesite	1.995	4.89±0.07	
17EC07	Pyr. andesite	1.326	5.06±0.07	
17EC08	Am. andesite	2.373	5.47±0.08	
17EC02	Pyr. andesite	1.219	6.47±0.09	Seaca-Tătarca
17EC01	Pyr. andesite	1.328	6.52±0.09	
17EC05	Pyr. andesite	1.517	6.61±0.09	
17EC04	Pyr. andesite	1.461	6.65±0.09	
17EC03	Pyr. andesite	1.193	6.79±0.10	
17KEL6	Px-Amph And.	1.680	8.33±0.12	Călimani
17P-KEL6	Px-Amph And.	1.648	8.30±0.12	
17KEL5	Monzodiorite	2.755	8.26±0.12	
17KEL1	Dacite	2.291	6.69±0.10	

Table 2. Volumetric data (computed from modelled volcanic uppermost surface) and growth rate for each of CGH volcano (labelled as in Fig. 1) and each CGH sectors (at bottom of the table). Values are quoted with uncertainties at 1σ-level. Constructed volume (V_C, in km^3), degree of denudation (D_{Den}): proportion of volcano lost by dismantling processes (in %). All morphometric values from this study except for Ciomadul volcano (Karátson et al., 2019)

Sector	Label and Volcanoes	**Radiometric data**			**Volumetric data**						
		$Age_{Beginning}$ (Ma)	$Age_{Endning}$ (Ma)	Lifespan (ΔT) (Ma)	Visible Area (km^2)	Height (m) a.base.l ± uncertainty (σZSV) (m)	Constructed volume (V_c in km^3)	Growth rate (GR) (km^3/Ma)	Eroded Volume (V_E in km^3)	Erosion rate (ER) (m /Ma)	Degree of Denudation (D_{Den})
Călimani	01 : Central Călimani (Kelemen)	10.6	6.7	3.9	1041	2072±82	592 ±115	152	158±85	17±9	27%
	02 : Moldoveanul (Moldovánka)	10.2	7.7	2.5	779	1053±78	320 ± 82	128	108±61	16±9	34%
Gurghiu	03 : Jirca (Nagy-Erdős)	9.2	8.4	0.8	137	1028±45	112 ±34	140	13±6	11±5	27%
	04 : Fâncel-Lăpuşna (Fancsal)	8.7	6.0	2.7	828	1499±58	355 ± 90	131	88±48	15±8	29%
	05 : Bacta (Bakta)	7.5	6.6	0.9	59	490±41	11 ± 6	12	3±2	7±6	32%
	06 : Seaca-Tătarca (Mezőhavas)	6.8	6.5	0.3	543	1650±63	248 ± 57	825	61±34	17±10	27%
	07 : Ciumani (Csomafalvi Délhegy)	7.1	6.3	0.8	106	1284±60	67 ± 18	84	9±6	12±9	18%
	08 : Borzont	-	-	-	59	493±45	21 ± 8	-	3±3	-	24%
	09 : Şumuleu (Somlyó)	6.7	6.2	0.5	242	1073±80	69 ± 25	138	12±19	8±12	18%
North Harghita	10 : Ostoroş (Osztoróc)	6.3	6	0.3	93	1008±37	49 ±16	163	6±3	10±6	20%
	11 : Ivo-Cocoizaş (Fertő-tető)	6.3	5.7	0.6	95	1104±57	55 ±16	92	7±5	12±10	23%
	12 : Râchitis (Csíkmagosa)	-	-	-	67	269±24	3 ± 3	-	1±2	-	21%
	13 : Vârghiş (Madarasi-Hargita)	5.5	4.6	0.9	355	1611±39	172 ± 34	191	25±14	14±8	16%
South Harghita	14 : Luci-Lazu (Nagykőbükk- Tetőfenyő)	4.3	3.6	0.7	306	843±74	108 ± 37	155	18±23	15±19	21%
	15 : Cucu (Kakukkhegy)	2.8	2.2	0.6	88	586±64	29 ± 11	49	5±6	22±26	20%
	16 : Pilişca (Piliske)	2.5	1.5	1.0	95	709±51	20 ± 8	20	3±5	18±26	17%
	17 : Central Ciomadul (Csomád)	0.2	0.03	0.2	72	-	7±1	37	0.2±0.1	26±4	3%

CGH sector	**Activity duration (Ma)**	**Total volume constructed per area (km^3)**	**Growth rates per area (km^3/Ma)**	**Degree of Denudation per sector (D_{Den} %)**	**Eroded volume (km^3)**	**Erosion rates (m/Ma)**
Călimani	3.9	910±140	235	30	265±105	17
Gurghiu	3.4	883±117	270	25	190±63	11
North Harghita	2.4	279±41	116	20	39±15	9
South Harghita	4.3	165±40	39	15	27±24	28
CGH total	**~11 Ma**	**2239±192**	**~200**	**~ 22**	**524±125**	**~20**

Table 3. Specific erosion rates along CGH range history for each contemporaneous climate period (details in Fig. 12 legend).

Sector	Period of activity (Ma)	Average age (Ma)	Erosion rate (m/Ma)	Climate fluctuation
Călimani	10.8 - 6.9	8.8	38	Short-time moderate period subtropical-continental transitional climate (More Humid; 3)
Gurghiu	8.7 - 5.5	7.1	14	Moderate continental climate (Less humid ; 2)
North Harghita and Luci-Lazu edifice	7- 4.6	5.8	7	Moderate continental climate with the identification of occasional semiarid condition (2)
South Harghita (Cucu, Pilişca, Ciomadul)	<3 - present	1.0	28	Moderate continental Humid condition with periglacial and minor glaciation (1)